Global Minimizers of Sigmoid Contrastive Loss

Kiril Bangachev[*‡]
kirilb@mit.edu

Guy Bresler[‡]
guy@mit.edu

Iliyas Noman
iliyas@mit.edu

Yury Polyanskiy[§]
yp@mit.edu

Department of Electrical Engineering and Computer Science
Massachusetts Institute of Technology
Cambridge, MA, 02139

Abstract

The meta-task of obtaining and aligning representations through contrastive pre-training is steadily gaining importance since its introduction in CLIP and ALIGN. In this paper we theoretically explain the advantages of synchronizing with *trainable inverse temperature and bias* under the sigmoid loss, as implemented in the recent SigLIP and SigLIP2 models of Google DeepMind. Temperature and bias can drive the loss function to zero for a rich class of configurations that we call (m, b_{rel})-Constellations. (m, b_{rel})-Constellations are a novel combinatorial object related to spherical codes and are parametrized by a margin m and relative bias b_{rel}. We use our characterization of constellations to theoretically justify the success of SigLIP on retrieval, to explain the modality gap present in SigLIP, and to identify the necessary dimension for producing high-quality representations. Finally, we propose a reparameterization of the sigmoid loss with explicit relative bias, which improves training dynamics in experiments with synthetic data. All code is available at RepresentationLearningTheory/SigLIP.

1 Introduction

Background. *Synchronizing representations* is an increasingly important meta-task in modern machine learning, appearing in several qualitatively different contexts. Models that operate jointly on visual and language data necessitate a synchronization of the representations of images and text [RKH+21, DKAJ21, SRC+21, CSDS21, JYX+21, LLXH22, SBV+22, BPK+22, ZWM+22, HGW+22, WYH+22, CWC+23, ZMKB23b, TGW+25b] and sometimes of additional modalities as well such as audio, thermal data, and others [GENL+23]. State-of-the-art vision models based on self-distillation rely on aligning the representations of augmentations of the same image [CKNH20a, HFW+20, CTM+21]. Likewise, aligning the representations of data produced by teacher and student networks [TKI20b, GS25] has been proposed as a method for distillation. Similarly to the teacher-student setup, the field of backward-compatible learning aims to synchronize the features produced by new models with features of already trained old models [RAVF+22, BPBDB23, SXXS20, JFF+23].

To mathematically formalize the task of synchronizing two representations, suppose that there are N data pairs $\{(X_i, Y_i)\}_{i=1}^N \in (\mathcal{X} \times \mathcal{Y})^{\otimes N}$. For concreteness, one can think of $\mathcal{X}$ as the space of images, $\mathcal{Y}$ as the space of text, and (X_i, Y_i) satisfy a *correspondence relation* such as the fact that they are a true image-caption pair. The goal is to train neural network *encoders* $f_\theta : \mathcal{X} \longrightarrow \mathbb{R}^d$ and $g_\phi : \mathcal{Y} \longrightarrow \mathbb{R}^d$ in such a way that the embeddings produced by them capture the correspondence relation. Such synchronization is usually achieved via minimizing a certain *contrastive loss*.

Despite the prevalence of the task of synchronizing representations, there is still limited understanding of *what loss function to use, how to choose its hyper-parameters*, and *what properties of the synchronized embeddings are desirable*. Theoretical results focus mostly on two loss functions – the InfoNCE loss [WI20, CRL+20, RCSJ21, EW22, LS22, PHD20, GRL+24] and the Sigmoid Loss [LCS24, LS22], which both depend on temperature and bias hyper-parameters. While these prior works have yielded useful insights, they leave important gaps in our understanding of representation synchronization:

1. Currently understood regimes for the number of represented objects N compared to the dimension of representations d do not reflect practice. To the best of our knowledge, in all prior theoretical works, either $d \geq N$, or N approaches $+\infty$ for a fixed value of d. As a comparison, the SigLIP2 model embeds text and images in $d \approx 10^3$ dimensions and operates with a dataset of size $N \approx 10^{10}$ [TGW+25b]. Thus the practically relevant regime – in which $d \ll N \ll 2^d$ – is not captured by prior work. The different regimes exhibit crucially different behaviors: practically relevant phenomena such as the *modality gap* [LZK+22] only arise when $N > d$, as we show in Theorem 3.6.

2. The optimal configurations identified by prior works are too rigid. For example, works in the regime $N \leq d$ typically suggest a simplex structure of the embeddings of each modality [EW22, LS22, LCS24]. This does not explain what the minimizing configurations are *when one modality is pretrained and locked*. In the regime $N \longrightarrow +\infty$, existing results typically suggest a perfect alignment between different representations. Again, this may be too stringent since it has been proposed that "different modalities may contain different information" [HCWI24]. In fact, empirical work suggests that even after synchronization, representations of text and images are completely disjoint, a phenomenon known as *the modality gap* [LZK+22, FMF25].

Our Contributions. In the current work, we address these gaps by analyzing the sigmoid loss *with trainable inverse temperature and bias parameters*, as used in Google's SigLIP models [ZMKB23b, TGW+25b] and Gemma 3 [TKF+25]. Making bias and temperature trainable is a key departure from prior theoretical work [WI20, LS22, EW22, LCS24] and leads to novel theoretical guarantees and practical recommendations. We first introduce the sigmoid loss and then describe our contributions.

The sigmoid loss for $U_i = f_\theta(X_i)$ and $V_i = g_\phi(Y_i)$ and inverse temperature[5] t and bias b is:

$$\mathcal{L}^{\mathsf{Sig}}(\theta, \phi; t, b) = \sum_{i=1}^N \log\left(1 + \exp(-t\langle U_i, V_i\rangle + b)\right) + \sum_{i \neq j} \log\left(1 + \exp(t\langle U_i, V_j\rangle - b)\right). \quad (1)$$

The first part of the loss encourages the embedding of an image and its caption to be similar, while the second part encourages mismatched image-caption pairs to be dissimilar.

1. The Geometry of Zero-Loss Configurations. Our work is the first to rigorously characterize global minima in representation synchronization tasks in the practical regime $N \gg d$.

We show that the SigLIP loss—with trainable temperature and bias—can be driven to zero by a rich family of solutions, which we fully characterize in terms of two novel geometric quantities – the *margin* $\mathsf{m} \geq 0$ and the *relative bias* $\mathsf{b_{rel}}$. Formally, a $(d, \mathsf{m}, \mathsf{b_{rel}})$-*Constellation*[6] $\{(U_i, V_i)\}_{i=1}^N \in \mathbb{S}^{d-1}$ is defined by the following inequalities:

Figure 1: Distribution of inner products between image and text embeddings from the ImageNet validation set using the $B/16$ 224×224 SigLIP model available at HuggingFace.

$$\langle U_i, V_i\rangle \geq \mathsf{m} + \mathsf{b_{rel}} \qquad \forall i,$$
$$\langle U_i, V_j\rangle \leq -\mathsf{m} + \mathsf{b_{rel}} \qquad \forall i \neq j. \quad (2)$$

---

[5]Previous works on synchronizing with sigmoid loss such as [ZMKB23b, TGW+25b, LCS24] call t the *temperature*. We call it *inverse temperature* to be more consistent with statistical physics terminology.

[6]We usually omit the parameter d since it is clear from the context and only write "$(\mathsf{m}, \mathsf{b_{rel}})$-constellation."
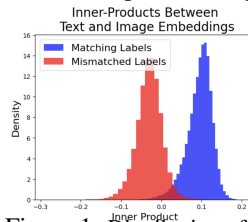
2

The existence of such $\mathsf{m}, \mathsf{b}_{\mathsf{rel}}$, which one can observe is equivalent to *the inner product separation* $\min_i \langle U_i, V_i \rangle \geq \max_{i \neq j} \langle U_i, V_j \rangle$, is a necessary and sufficient condition for $\{(U_i, V_i)\}_{i=1}^N$ to be a global minima of the sigmoid loss with trainable inverse temperature and bias. We show that this is nearly satisfied in practice for the SigLIP model trained on real images and text – See Figure 1[7]. Surprisingly, any configuration satisfying this condition is also a global minimum for the *triplet loss*, see Observation 4. We interpret the margin and relative bias in Section 3.1.

In practice, one needs to choose a dimension for the encoders which has large enough "capacity" to hold the embeddings of great many pairs U_i, V_i. However, despite intuitive notion that capacity should increase with dimension, to the best of our knowledge no such quantitative characterization was available before our work. Formally, we define the following combinatorial problem and make partial progress in Section 3.2 via a connection to spherical codes.

Problem 1. *For a given* $\mathsf{m} \geq 0, \mathsf{b}_{\mathsf{rel}} \in [-1, 1]$, *find the largest number of points* $N = \mathsf{N}_{\mathsf{MRB}}(d, \mathsf{m}, \mathsf{b}_{\mathsf{rel}})$ *such that there exist* $2N$ *vectors* $\{(U_i, V_i)\}_{i=1}^N \in \mathbb{S}^{d-1}$ *satisfying* (2).

2. Success of Zero-Loss Configurations on Downstream Tasks.

In Corollary 1, we use the characterization of zero-loss configurations to show that a standard nearest neighbor search on *any* $(\mathsf{m}, \mathsf{b}_{\mathsf{rel}})$-*Constellation gives perfect retrieval*, even though typically there is no perfect alignment between the two representations. Increasing the margin m of a constellation makes retrieval robust to larger approximation errors. This is important in practice since retrieval is often performed via an *approximate nearest neighbor search* for computational efficiency [XXL+21, KZ20, MT21].

Figure 2: Region of possible $(\mathsf{m}, \mathsf{b}_{\mathsf{rel}})$-Constellations. In red is the impossible region, in which no large configurations are possible (Theorem 3.4). In green is the region where constellations of exponential size exist (Theorem 3.3 and Theorem 3.5). In the shaded region we prove that a modality gap exists (Theorem 3.6).

3. The Modality Gap: Synchronize, do not Align.

The analysis of [WI20] suggests alignment between representations when training via the InfoNCE loss – the representations of the word "cat" and the image of a cat should (nearly) coincide. Yet, it has been empirically observed that there is a *modality gap* [LZK+22, FMF25]. The representations of images and text – synchronized via the InfoNCE loss in CLIP – do not align, but rather belong to fully disjoint, linearly separable regions. Furthermore, this is not caused by the difference between architecture of image and text encoders, as initially thought, but rather directly by virtue of (approximately) minimizing InfoNCE loss [FMF25].

We shed light on this empirical discovery and prove in Theorem 3.6 that linear separability between modalities holds for any zero-loss configuration of the sigmoid loss in the practically relevant regime $N > d$ when $|\mathsf{b}_{\mathsf{rel}}| < \mathsf{m}$ (Figure 2). We verify our findings by performing experiments with 8 different SigLIP models from Hugging Face on the ImageNet dataset (models given in Table 1). We observe perfect linear separability of image and text embeddings for all models. From a philosophical point of view, as "different modalities may contain different information" [HCWI24], it is only natural that they be represented in disjoint parts of the space.

We leverage the modality gap to build a linear adapter which can be used towards synchronizing representations when one encoder is locked. This is the reason why we use the name *representation synchronization* rather than representation alignment: alignment between modalities is neither achieved nor desired.

Figure 3: Modality gap in SigLIP on ImageNet data with the B/16 model with 224×224 resolution. We find a perfect linear separator using the perceptron algorithm.

4. Implications of The Solution Geometry in Practice: Relative Bias Parameterization of Sigmoid Loss.

We propose a parametrization of the sigmoid loss that depends on the *relative bias* rather than the bias in Definition 1. The relative bias parametrization has the following advantages:
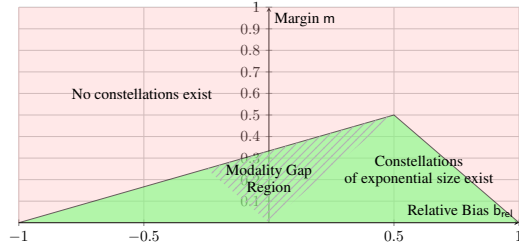
---

[7]The experimental details for all plots as well as further experiments are in Section D.

1. Locked Representation: For example, in LiT [ZWM$^+$22], the image encoder is already trained and locked and we want to synchronize the text encoder with it. The sigmoid loss with trainable parameters in the relative bias parametrization allows us to find a zero-loss configuration for text and images *regardless* of the image encoder. In Observation 1, we show that trainable relative bias and inverse temperature provide a mechanism to implicitly add linear adapters on top of the two encoders as in Figure 4. The linear adapters can alternatively be used for synchronizing with a locked modality. The adapters we propose in Observations 1 and 2 extend the *Double-Constant Embedding Model* of [LCS24].

2. More than Two Modalities: The framework of training with the relative bias parameterization also leads to theoretical guarantees for the global minima of synchronizing more than two modalities via the sigmoid loss. Again, in Observation 2 we show that the parameterization implicitly captures the addition of a modality-dependent linear adapter to each encoder.
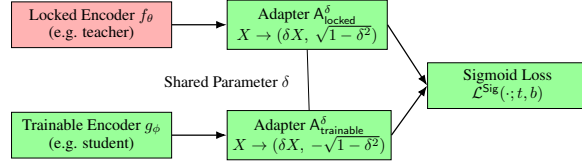

Figure 4: Implicit adapter in relative bias parameterization of sigmoid loss with a locked representation. The parameters ϕ, δ, t, b in green blocks are trainable. Parameter θ is locked.

3. Guiding Relative Bias: Relative bias and margin, which are related by inequalities that we fully characterize in Theorems 3.3 and 3.4, control important properties of the synchronized representations such as *retrieval robustness* and *the presence of a modality gap*. We observe empirically that in the usual sigmoid loss parameterization, Adam [KB15] finds configurations with a zero relative bias, thus limiting the set of trained representations. By adding a relative bias parameter and locking it, we can provably guide the zero loss configuration to a more diverse set of solutions. See Section D.4.

2 Background and Prior Work

Representation Learning And Synchronization. A key insight in [RKH$^+$21, JYX$^+$21] is that training a model to *simultaneously* operate on multiple modalities (such as image and text) enables SOTA performance on individual modalities as well – "if you want to train the best vision model, you should train not just on N images but also on M sentences" [HCWI24]. Several empirical approaches towards synchronizing multiple representations have been proposed, including CLIP [RKH$^+$21], BLIP [LLXH22], ALIGN [JYX$^+$21], LiT [ZWM$^+$22], and SigLIP [ZMKB23b, TGW$^+$25b]. The task of synchronizing representations goes beyond synchronizing across different modalities such as image and text, but also includes synchronizing the representations of a student model to a teacher model with the purpose of distillation [TKI20b, GS25] and self-distillation [CTM$^+$21], and aligning the representations of data augmentations [ZIE$^+$16, NF16, GSK18, CKNH20a, HFW$^+$20, CTM$^+$21].

Formalizing Representation Synchronization. In this paper, we consider unit-norm encoders $f_\theta : \mathcal{X} \longrightarrow \mathbb{S}^{d-1}, g_\phi : \mathcal{Y} \longrightarrow \mathbb{S}^{d-1}$ (unit norm representations are predominant in practice, see e.g. [SKP15, PVZ15, LWY$^+$17, WXCY17, CKNH20b, HFW$^+$20, TKI20a, ZMKB23b, TGW$^+$25b] and others). Synchronizing the representations produced by f_θ, g_ϕ is usually achieved via minimizing a certain loss function $\mathcal{L}$ over the kernel produced by the embeddings:

$$\mathcal{L}(\theta, \phi; \Gamma) = \mathcal{L}(\{\langle f_\theta(x_i), g_\phi(y_j)\rangle\}_{1\leq i,j\leq N}; \Gamma) \tag{3}$$

where Γ is a set of hyper-parameters, typically involving (inverse) temperature and bias. The optimization is performed via batch first-order optimization methods such as SGD or Adam [KB15].

Depending on the targeted representations, one may choose the parameters over which the optimization is performed. If both f_θ, g_ϕ are untrained, one may perform gradient descent on both ϕ, θ in (3) as in CLIP [RKH$^+$21]. On the other hand, if one of the models – say f_θ – is already trained and trusted (for example, because it is the teacher model that we are trying to distill [CTM$^+$21, GS25]), we do not update its parameters or only update a small adapter on top of it as in [ZZF$^+$22, LXGY23, GGZ$^+$24, YZWX24, LHY$^+$24, EANP24]. Likewise, this is the case when one of the modalities has already been trained and is locked [ZWM$^+$22, RNP$^+$22, LLXH22, LLSH23].

4

Besides choosing which parameters to update, one also needs to choose a concrete loss function $\mathcal{L}$. The choices depend on two factors: 1) What is the geometry of the desired minimizing configurations of representations? 2) How efficient is the computation of the loss in terms of the batch size?

We focus on two different loss functions – InfoNCE and sigmoid – and now survey previous works on them. In order to understand the solution geometry of the minimizers, a typical assumption is that the underlying networks f_θ, g_ϕ are sufficiently expressive and can encode any embedding $\{(U_i, V_i)\}_{i=1}^N = \{(f_\theta(X_i), g_\phi(Y_i))\}_{i=1}^N$ [WI20, EW22, LS22, LCS24]. We also adopt this approach.

Solution Geometry with InfoNCE. The InfoNCE loss [vdOLV19] with inverse temperature $t > 0$ and bias b is a special case of (3) and takes the following form

$$\mathcal{L}^{\mathsf{InfoNCE}}(\{(U_i, V_i)\}_{i=1}^N; t) = -\frac{1}{N} \sum_{i=1}^N \log \frac{\exp(t\langle U_i, V_i\rangle)}{\sum_j \exp(t\langle U_i, V_j\rangle)} - \frac{1}{N} \sum_{i=1}^N \log \frac{\exp(t\langle U_i, V_i\rangle)}{\sum_j \exp(t\langle U_j, V_i\rangle)}.$$

(4)

It effectively takes a soft-max over all the rows and columns of the matrix $tU^T V$, an interpretation that yields a connection to the InfoMax principle [HFLM$^+$19] as well as to maximizing point-wise mutual information [TKI20a] and approximate sufficient statistics [OLCM25, LM25].

The solution geometry has been characterized in the case $d \geq N + 1$. The global minimum loss is achieved when $U_i = V_i$ for each i and $U_1, U_2, \ldots, U_n$ form a simplex [EW22, LS22]. When $N \longrightarrow +\infty$, the minimizing measures converge to perfectly aligned ($U_i = V_i$ for all i) and uniform (the discrete measure corresponding to $\{U_i\}_{i=1}^n$ converges weakly to the uniform measure). Several works including [SPA$^+$19, EG24] take a different direction and analyze the global minima of the InfoNCE loss (and its symmetrization SimCLR) in terms of performance on downstream (linear) classification tasks instead. While such a geometric characterization is appealing from a practical point of view, these works also do not address the aforementioned gaps in our understanding. The results of [SPA$^+$19] hold in the regime $N \longrightarrow +\infty$ and [EG24] points out that "temperature scaling in the SimCLR loss remains challenging."

In a very different direction, recently it was also rigorously shown that the InfoNCE yields an optimal dimensionality reduction with input data from a Gaussian Mixture Model [BKS25].

Solution Geometry with Sigmoid Loss. An alternative loss function used towards alignment is the sigmoid loss [ZMKB23b, TGW$^+$25b] defined in (1). One advantage of the sigmoid loss over InfoNCE is that it does not have a batch normalization term such as $\sum_{j \neq i} \exp(t\langle U_i, V_j\rangle - b)$ and, thus, every pair (U_i, V_j) can be processed separately. This allows for parallel computation.

The solution geometry of configurations achieving global minimum loss has been characterized when $d \geq N$ [LCS24]. For a simplex $\{W_i\}_{i=1}^N$ in $\mathbb{S}^{d-2}$ and some $\delta \in [0, 1]$, it holds that $U_i = (\delta W_i, \sqrt{1 - \delta^2}), V_i = (\delta W_i, -\sqrt{1 - \delta^2})$ for each i, where the value of δ depends on the relationship between t and b. In most cases, either the representations collapse to perfectly aligned ($\delta = 1$ and $U_i = V_i$ for all i) or antipodal ($\delta = 0$ and $U_i = -V_i = (1, 0, 0 \ldots, 0)$ for all i). The construction of [LCS24] is the basis for several of our results, including the adapters proposed in Observations 1, 2.

Other loss functions. Loss functions such as the triplet loss [SKP15] and f-MICl [LZS$^+$23] have also been considered. We further discuss the triplet loss in Section A.3.

3   Main Results

3.1   Geometric Characterization of Zero Loss Representations

In (1), $\mathcal{L}^{\mathsf{Sig}}(\{(U_i, V_i)\}_{i=1}^N; t, b) \geq 0$ holds for any inputs because $\log(1 + e^\kappa) \geq 0$ for any $\kappa \in \mathbb{R}$. Hence, global minimizers are any choice of representations and parameters $\{(U_i, V_i)\}_{i=1}^N; t, b \in (\mathbb{S}^{d-1})^{\otimes N} \times (\mathbb{S}^{d-1})^{\otimes N} \times [0, +\infty] \times [-\infty, \infty]$ leading to a zero loss. We characterize such configurations fully in the following theorems. The proofs are simple and delayed to Section A.

Theorem 3.1 (All Global Minima are $(\mathsf{m}, \mathsf{b_{rel}})$-Constellations). *Suppose that any iterative algorithm produces a sequence $\{U_i^{(s)}\}_{i=1}^N, \{V_i^{(s)}\}_{i=1}^N, t^{(s)} > 0, b^{(s)}$ for $s = 1, 2, \ldots$ such that*

$$\lim_{s \longrightarrow +\infty} \mathcal{L}^{\mathsf{Sig}}(\{U_i^{(s)}\}_{i=1}^N, \{V_i^{(s)}\}_{i=1}^N; t^{(s)}, b^{(s)}) = 0.$$

Then, there exists some subsequence indexed by $(s_r)_{r=1}^{+\infty}$ such that

$$\lim_{r \longrightarrow +\infty} U_i^{(s_r)} = U_i, \quad \lim_{r \longrightarrow +\infty} V_i^{(s_r)} = V_i \text{ for all } i, \quad \lim_{r \longrightarrow +\infty} \frac{b^{(s_r)}}{t^{(s_r)}} = \mathsf{b_{rel}}, \tag{5}$$

and there exists some $\mathsf{m} \geq 0$ such that $\{(U_i, V_i)\}_{i=1}^N, \mathsf{m}, \mathsf{b_{rel}}$ satisfy (2).

Theorem 3.2 (All $(\mathsf{m}, \mathsf{b_{rel}})$-Constellations Are Global Minimizers). *Suppose that $\{(U_i, V_i)\}_{i=1}^N \in \mathbb{S}^{d-1}$ satisfies (2) for some $\mathsf{m} > 0$. If we set $b = \mathsf{b_{rel}} \times t$, then*

$$\lim_{t \longrightarrow +\infty} \mathcal{L}(\{U_i\}_{i=1}^N, \{V_i\}_{i=1}^N; t, \mathsf{b_{rel}} \times t) = 0.$$

Moreover, for $\mathsf{m}^* := \frac{1}{2}(\min_i \langle U_i, V_i \rangle - \max_{i \neq j} \langle U_i, V_j \rangle)$, $\mathsf{b_{rel}^*} := \frac{1}{2}(\min_i \langle U_i, V_i \rangle + \max_{i \neq j} \langle U_i, V_j \rangle)$,

$$\inf_b \mathcal{L}^{\mathsf{Sig}}(\{U_i\}_{i=1}^N, \{V_i\}_{i=1}^N; t, b) = e^{-t\mathsf{m}^* + o(t)}$$

and is achieved when $b = \mathsf{b_{rel}^*} \times t + o(t)$.

Table 1: Margin and Relative bias corresponding to 5th-percentile positive and 95-th percentile negative pairs for different SigLIP models. We highlight that the two largest so400m models have a substantially different relative bias than the rest of the models. Likewise, the margin is perfectly correlated with the embedding dimension – bigger models have bigger margin.

Model	5% Positive Pairs	95% Negative Pairs	Margin	Relative Bias	Dimension
siglip-so400m-patch14-384	0.0769	0.0486	0.0142	0.0627	1152
siglip-so400m-patch14-224	0.0747	0.0483	0.0132	0.0615	1152
siglip-large-patch16-256	0.0400	0.0151	0.0124	0.0276	1024
siglip-large-patch16-384	0.0353	0.0120	0.0117	0.0237	1024
siglip-base-patch16-512	0.0409	0.0170	0.0120	0.0289	768
siglip-base-patch16-384	0.0408	0.0173	0.0118	0.0290	768
siglip-base-patch16-256	0.0413	0.0200	0.0106	0.0306	768
siglip-base-patch16-224	0.0383	0.0181	0.0101	0.0282	768

This characterization is for global minima in the case of zero loss, which may seem too idealistic. However, it turns out that practically trained models are (up to a small error) also Constellations. In Table 1, we provide the optimal relative bias and margin after removing 5% outliers from the positive and negative pairs.

It turns out that $(\mathsf{m}, \mathsf{b_{rel}})$-constellations are also global minimizers for the triplet loss, which is another popular contrastive training objective [SKP15], see Section A.

Theorem 3.2 shows not only that any $(\mathsf{m}, \mathsf{b_{rel}})$-constellation is a global minimizer, but also that *the optimal margin m^* characterizes the speed of convergence of the loss to zero.*

Any $(\mathsf{m}, \mathsf{b_{rel}})$-Constellation yields perfect retrieval follows as a corollary of Theorem 3.1. In the image-text retrieval task, one is given an image (respectively text) and has to produce the text (respectively image) that best matches it. In our mathematical model, this corresponds to producing U_i on input V_i (and V_i on input U_i).

Corollary 1 (Nearest Neighbor Search Yields Perfect Retrieval). *Suppose that $\{(U_i, V_i)\}_{i=1}^N$ is a zero loss configuration. Then, a nearest neighbor of U_i among $\{V_j\}_{j=1}^N$ is V_i. If, furthermore, the margin m is strictly positive, this neighbor is unique.*

In practice, retrieval is often performed via *approximate* nearest neighbor search [XXL+21, KZ20, MT21] as this approach has significant computational efficiency advantages. Hence, representations more robust to approximation errors are more desirable. Since $\min_i \langle U_i, V_i \rangle - \max_{i \neq j} \langle U_i, V_j \rangle \geq$

6

2m when (2) is satisfied, representations with a larger margin are more robust. The importance of margin on retrieval has been empirically observed and exploited in several empirical works [LWYY16, DGY$^+$22]. Corollary 1 is for perfect zero-loss constellations. A more robust version also holds, which is closer to practice due to the fact that practical models *are not trained to zero loss* (and cannot be, both due to computational limitations and mislabeled data). We note that in the basic version of the proposition, one can ignore batch size and take $B = N$. We also include the effect of batch size since this is how models are trained in practice.

Proposition 1 (Robustness of Retrieval via Nearest Neighbor Search). *Let the embedded dataset be* $\{(U_i, V_i)\}_{i=1}^N$. *Suppose that for inverse temperature and bias* $t > 0, b$ *and some* $\xi \in [0, 1]$, *and some batch size* $N > B > \sqrt{N}$, *it holds that:*[8]

$$\underset{(a_j)_{j=1}^B \sim [N]^{\times k}}{\mathbb{E}} \Big[\sum_{j=1}^B \log \Big(1 + \exp(-t\langle U_{a_j}, V_{a_j}\rangle + b) \Big)$$
$$+ \sum_{i \neq j} \log \Big(1 + \exp(t\langle U_{a_i}, V_{a_j}\rangle - b) \Big) \Big] \leq \xi \log 2.$$

Then, for at least a $1 - \frac{N\xi}{B(B-1)}$ *fraction of the values* U_i *(respectively,* V_i*), a nearest neighbor search returns* V_i *(respectively,* U_i*).*

The proof is delayed to Section A.2. Note that while $N > B > \sqrt{N}$ is restrictive, it is relevant to models trained with massive compute. For example, in [ZMKB23b], the authors run models with batch sizes up to 64000 which makes the statement meaningful for datasets of size as large as 10^{10}.

3.2 Constructions of $(d, \mathsf{m}, \mathsf{b_{rel}})$-Constellations And Cardinality Bounds

Our results so far are vacuous if no $(\mathsf{m}, \mathsf{b_{rel}})$-Constellations exist. In this section, we show a generic construction which is largely motivated by the Double-Constant Embedding Model of [LCS24] but replaces the simplex with a *spherical code*. For $\alpha \in [-1, 1)$ and $d \in \mathbb{N}$, a (d, α)-spherical code is a collection of vectors $X_1, X_2, \ldots, X_N \in \mathbb{S}^{d-1}$ such that $\langle X_i, X_j \rangle \leq \alpha$ for all $i \neq j$ [CSB$^+$13, (52)]. In particular, any (d, α) code is a $(d, \frac{1-\alpha}{2}, \mathsf{b_{rel}} = \frac{1+\alpha}{2})$-constellation and vice-versa. This implies that any construction of spherical codes immediately implies a construction of $(\mathsf{m}, \mathsf{b_{rel}})$-Constellations when $\mathsf{m} + \mathsf{b_{rel}} = 1$. Spherical codes are a well-studied object in combinatorics and many constructions exist depending on α (see [CSB$^+$13] and references therein). The following construction shows that we can extend to the case when $\mathsf{m} + \mathsf{b_{rel}} \neq 1$.

Construction 1 (Construction of $(\mathsf{m}, \mathsf{b_{rel}})$-Constellations). *Consider any* $(d-2, \mathsf{m}, \mathsf{b_{rel}})$-*constellation* $\{(U_i, V_i)\}_{i=1}^N$. *Then, for any* $\delta, \phi \in [0, 1)$ *such that* $\delta^2 + \phi^2 \leq 1$, *the following vectors form a* $(d, \mathsf{m}', \mathsf{b_{rel}}')$-*constellation with* $\mathsf{m}' = \delta^2 \mathsf{m}$ *and* $\mathsf{b_{rel}}' = \delta^2 \mathsf{b_{rel}} + \phi^2 - (1 - \delta^2 - \phi^2)$:

$$U_i' = (\delta U_i, \phi, \sqrt{1 - \delta^2 - \phi^2}) \qquad and \qquad V_i' = (\delta V_i, \phi, -\sqrt{1 - \delta^2 - \phi^2}). \tag{6}$$

This construction shows that $(\mathsf{m}, \mathsf{b_{rel}})$-Constellations not only exist but constitute a rich family. One can in fact construct them from any locked $(d - 2)$-dimensional embedding $\{X_i\}_{i=1}^N$ as long as $X_i \neq X_j$ for $i \neq j$ which is the basis of our algorithm for synchronizing with a locked encoder in Observation 1. Recall that the margin impacts the robustness of the representation for retrieval. Thus, it is of both practical and theoretical interest to analyze how large the margin could be for a given dimension d and sample size N. Construction 1 immediately gives a recipe for this based on spherical code bounds.
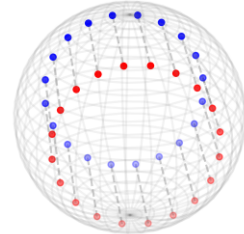

Figure 5: 3D visualization of configurations in Example 3, obtained by minimizing sigmoid loss with Adam; each (U_i, V_i) pair is a reflection across a hyperplane.

That is, let $\mathsf{N_{SC}}(d, \alpha)$ be the largest possible size of a (d, α)-spherical code. Let $\mathsf{E_{SC}}(\alpha) = \liminf_{d \to +\infty} \frac{\log \mathsf{N_{SC}}(d, \alpha)}{d}$. Determining $\mathsf{N_{SC}}, \mathsf{E_{SC}}$ is a well studied problem in coding theory [CSB$^+$13]. We similarly define the numbers $\mathsf{N_{MRB}}(d, \mathsf{m}, \mathsf{b_{rel}})$ and $\mathsf{E_{MRB}}(\mathsf{m}, \mathsf{b_{rel}})$ for the largest $(\mathsf{m}, \mathsf{b_{rel}})$-constellations in dimension d. Construction 1, together with the classical bound $\mathsf{E_{SC}}(\alpha) \geq \log_2 \frac{1}{\sqrt{1-\alpha^2}}$ due to Shannon [Sha59] and Wyner [Wyn68] implies:

---

[8] We denote by $[N]^{\times B}$ the uniform distribution over B-tuples in $[N]$ of distinct indices.

Theorem 3.3 (Lower Bound on the Size of Constellations). *Suppose that* $m \geq 0, b_{rel} \in [-1,1]$ *satisfy* $m + b_{rel} < 1$ *and* $3m < 1 + b_{rel}$. *Then, there exist* (m, b_{rel})-*constellations of size exponential in dimension and furthermore*

$$\mathsf{E}_{\mathsf{MRB}}(m, b_{rel}) \geq \mathsf{E}_{\mathsf{SC}}\left(\frac{1 + b_{rel} - 3m}{1 + b_{rel} + m}\right) \geq -\frac{1}{2}\log_2\left(1 - \left(\frac{1 + b_{rel} - 3m}{1 + b_{rel} + m}\right)^2\right).$$

Proof. Let $\alpha := \frac{1+b_{rel}-3m}{1+b_{rel}+m} \in [0,1]$. Let $X_1, X_2, \ldots, X_N$ be an α-spherical code in dimension $d-2$ of size $\exp\left((d-2)(\mathsf{E}_{\mathsf{SC}}(\alpha) + o(1))\right) = \exp\left(d(\mathsf{E}_{\mathsf{SC}}(\alpha) + o(1))\right)$. Choose ϕ, δ as follows:

$$\delta^2 = \frac{2m}{1-\alpha}, \qquad \phi^2 = \frac{2b_{rel} + 2 - \delta(3 + \alpha)}{4}.$$

One can easily check that the inequalities $m + b_{rel} \leq 1$ and $3m \leq 1 + b_{rel}$ imply that these values are well-defined in the sense that $\delta^2 > 0, \phi^2 > 0$ and, furthermore, $\delta^2 + \phi^2 \leq 1$. Now, we can apply Construction 1 with $U_i = V_i = X_i$ and δ, ϕ and conclude the desired result. $\square$

The conditions $m + b_{rel} \leq 1$ and $3m \leq 1 + b_{rel}$ are not a virtue of our construction, but turn out to be necessary via an argument resembling Rankin's proof that among any $k + 1$ vectors in $\mathbb{S}^{d-1}$, there exist two with inner product at least $-\frac{1}{k}$ [Ran55]. We actually manage to prove a lower bound for a more general set of configurations than constellations.

Theorem 3.4 (Upper Bounds on Margin via Relative Bias). *Suppose that* $\{(U_i, V_i)\}_{i=1}^N$ *satisfy that* $\frac{1}{N}\sum_i \langle U_i, V_i \rangle \geq m + b_{rel}$ *and* $\frac{1}{N(N-1)}\sum_{i \neq j}\langle U_i, V_j \rangle \leq -m + b_{rel}$ *(in particular, this holds for any* (m, b_{rel})-*constellation). Then, it also holds that*

$$m + b_{rel} \leq 1 \quad and \quad 3m \leq 1 + b_{rel} + o(1).$$

Proof. The inequality $m + b_{rel} \leq 1$ is trivial since $m + b_{rel} \leq \max\langle U_1, V_1 \rangle \leq \max \|U_1\|_2 \times \|V_1\|_2 \leq 1$ by (2) and Cauchy-Schwarz. For the second inequality, we use the following fact from [LCS24]. For any unit vectors $\{(U_i, V_i)\}_{i=1}^N$, it holds that

$$\frac{1}{N^2}\sum_{i \neq j}\langle U_i, V_j \rangle \geq \frac{N-2}{2N^2}\sum_i \langle U_i, V_i \rangle - \frac{1}{2}.$$

Using $\langle U_i, V_j \rangle \leq b_{rel} - m, \langle U_i, V_i \rangle \geq b_{rel} + m$ gives $(3 - \frac{4}{N})m \leq 1 + b_{rel}$. $\square$

We also provide upper bounds on the size of a constellation given the margin m. This can be used to inform the size of the embedding space given the number of pairs (U_i, V_i) we want to embed in it.

Theorem 3.5 (Upper Bound on the Size of Constellations). *Suppose that* $\{(U_i, V_i)\}_{i=1}^N$, *is a* (m, b_{rel})-*constellation for some* $m \geq 0, b_{rel} \in [-1,1]$ *which satisfy* $m + b_{rel} \leq 1$ *and* $3m \leq 1 + b_{rel}$. *Then,*

$$N \leq \exp\left(-d\frac{1}{2}\log\left(1 - \frac{1 + b_{rel} - 3m}{1 + b_{rel} + m}\right) + o(d)\right).$$

Equivalently,

$$\mathsf{E}_{\mathsf{MRB}}(m, b_{rel}) \leq -\frac{1}{2}\log\left(1 - \frac{1 + b_{rel} - 3m}{1 + b_{rel} + m}\right).$$

The proof is delayed to Section B. We plot the upper and lower bounds from this section in Figure 6 for $b_{rel} = 0$ and $m = 0.1$. In Section E, we note that the proof also illustartes a connection with the linear representation hypothesis, e.g. [PCV24].

We note that in [RCSJ21, Theorem 4], the authors find a different connection between spherical codes and minimizers of the InfoNCE loss. In the recent work [WBNL25], the authors show a different dimension lower-bound for existence of vector embeddings for top-k retrieval.

We end with zooming into the Figure 2 and plotting the performance of several trained siglip
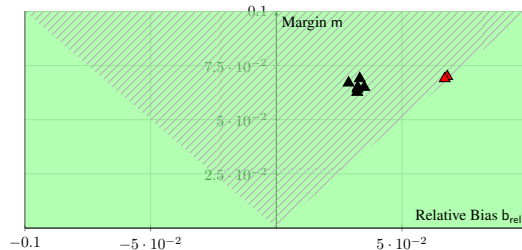

Figure 7: Mean inner products of positive pairs $\langle U_i, V_i \rangle$ versus mean inner products of negative pairs $\langle U_i, V_j \rangle$ from the ImageNet validation dataset.
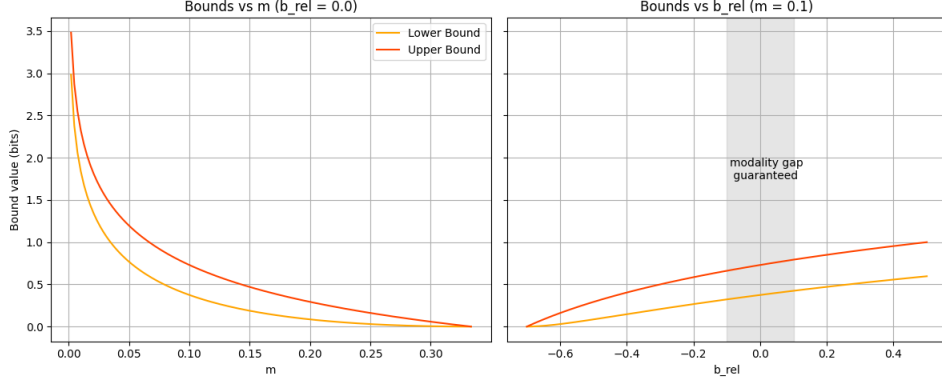
8

Figure 6: Upper and Lower Bounds from Theorem 3.5 and Theorem 3.3 for fixed $\mathsf{b}_{\mathsf{rel}} = 0$, $m = 0.1$.

models from Hugging Face. We observe two clusters – one composed of the larger so400m models (around 1B parameters) and another cluster of smaller models (up to .4B). It is interesting to consider that the so400m are exactly on the boundary where the modality gap is guaranteed (all 8 models do satisfy the modality gap with zero misclassification error). The differnece in margins is partly explained by dimensionality – larger dimensions correspond to larger margins. The Pearson correlation coefficient between dimension and margin is .948 and the Spearman coefficient is .926.

Table 2: Mean cosine similarities, margin, and relative bias for different SigLIP models.

Model	Mean Pos. Pairs	Mean Neg. Pairs	Margin	Relative Bias	Dimension
siglip-so400m-patch14-384	0.1376	-0.0015	0.0695	0.0680	1152
siglip-so400m-patch14-224	0.1365	-0.0022	0.0694	0.0672	1152
siglip-large-patch16-256	0.1023	-0.0359	0.0691	0.0332	1024
siglip-large-patch16-384	0.0958	-0.0384	0.0671	0.0287	1024
siglip-base-patch16-256	0.1004	-0.0294	0.0649	0.0355	768
siglip-base-patch16-512	0.0971	-0.0322	0.0646	0.0324	768
siglip-base-patch16-384	0.0966	-0.0319	0.0642	0.0324	768
siglip-base-patch16-224	0.0950	-0.0305	0.0627	0.0322	768

3.3 The Modality Gap in SigLIP

The construction in Example 1 satisfies the modality gap property – when $\delta > 0$, the representations of the two modalities are separated by a hyperplane (orthogonal to the last coordinate). This phenomenon appears not only in our construction, but has been observed empirically on synchronized text and image embeddings in CLIP [LZK$^+$22, FMF25] and in SigLIP by us in Figure 3. We show a rigorous justification for this.

Theorem 3.6 (Modality Gap in Zero-Loss Configurations). *Suppose that $N \geq d + 2$ and $\{(U_i, V_i)\}_{i=1}^N$ are such that $\langle U_i, V_i \rangle > 0$ for all i, $\langle U_i, V_j \rangle < 0$ for all $i \neq j$. This happens for example, when $\mathsf{m} > |\mathsf{b}_{\mathsf{rel}}|$ in a $(\mathsf{m}, \mathsf{b}_{\mathsf{rel}})$-Constellation. Then, there exists some $h \in \mathbb{S}^{d-1}$ such that:*

$$\langle h, U_i \rangle > 0 \qquad \text{for all } i, \tag{7}$$
$$\langle h, V_j \rangle < 0 \qquad \text{for at least } N - d \text{ values of } j. \tag{8}$$

The fact that the condition (8) is satisfied for at least $N - d$ values of j instead of all N is rather minor in practice. As mentioned, in SigLIP2 [TGW$^+$25b], $N \approx 10^{10}$ and $d \approx 10^3$. Thus, our result shows the modality gap holds for all but .0000001% of the text embeddings. We note that the theorem is essentially tight – in Example 3, we show an example in which $d - 1$ of the vectors V_j cannot be separated from the vectors U_i. We also note that $\mathsf{m} > |\mathsf{b}_{\mathsf{rel}}|$ is also plausible as practically trained models such as SigLIP2 have a small relative bias of magnitude less than 0.1 [ZMKB23a].

9

Proof Sketch. The full proof is in Section C, where we also analyze further properties of configurations satisfying (7) and (8). Here we give a sketch. First, we use Helly's theorem (Theorem C.1) to show that the convex sets $\{x : \langle x, U_i \rangle > 0\}_{i=1}^{N}$ have a non-empty intersection and, hence, there exists some $h \in \mathbb{S}^{d-1}$ such that $\langle h, U_i \rangle > 0$ for each i. Then, we use the hyperplane separation theorem (Theorem C.3) to show that the projection $\bar{h}$ of h on the convex cone defined by $U_1, U_2, \ldots, U_N$ also has this property. Finally, we use Caratheodory's theorem (Theorem C.2) to show that $\bar{h}$ has a positive inner product with all the vectors U_i and is in the convex cone of at most d of the vectors U_j. This implies that $\bar{h}$ has a negative inner product with all the other $N - d$ vectors V_k. $\qquad\square$

3.4 Experiments: Sigmoid Loss with Explicit Relative Bias Parameterization

Due to the importance of the relative bias parameters for global minima of sigmoid loss, we propose a parameterization that explicitly captures this dependence.

Definition 1 (Parameterization with Explicit Relative Bias)**.** *The relative bias parametrization of the sigmoid loss for encoder* f_θ, g_ϕ *over data pairs* $\{(X_i, Y_i)\}_{i=1}^{N}$ *with* $U_i = f_\theta(X_i), V_i = g_\phi(Y_i)$ *is*

$$
\begin{aligned}
&\mathcal{L}^{\mathsf{RB-Sig}}(\theta, \phi; t, \mathsf{b_{rel}}) \\
&= \sum_{i=1}^{N} \log\left(1 + \exp(-t\langle U_i, V_i \rangle + t\mathsf{b_{rel}})\right) + \sum_{i \neq j} \log\left(1 + \exp(t\langle U_i, V_j \rangle - t\mathsf{b_{rel}})\right).
\end{aligned}
\tag{9}
$$

Figure 8: Evolution of margins when training with different fixed relative biases, average over 100 iterations.

Clearly, $\mathcal{L}^{\mathsf{RB-Sig}}(\theta, \phi; t, \mathsf{b_{rel}}) = \mathcal{L}^{\mathsf{Sig}}(\theta, \phi; t, \mathsf{b_{rel}} \times t)$ so the loss functions are the same. However, we show that running Adam [KB15] on $\mathcal{L}^{\mathsf{RB-Sig}}$ yields faster convergence – see Figures 10 and 11. It also provides the additional flexibility to freeze the relative bias to a desired value and only train inverse temperature. This may be important since we observe that in practice relative bias converges to 0 when not frozen. For example, in SigLIP2 [ZMKB23a] with the B/16 model with resolution 384×384, we have learned parameters $t \approx 117.8, b \approx -12.9$, so $\mathsf{b_{rel}} \approx -0.11$. We give further experimental evidence for this in Section D.4. Thus, we propose using our parameterization $\mathcal{L}^{\mathsf{RB-Sig}}$ in practice over $\mathcal{L}^{\mathsf{Sig}}$.
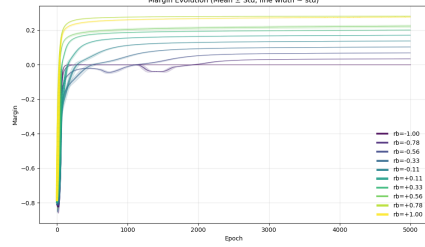
Fixed Relative Bias. One functionality that this new parameterization gives us is to train models with a fixed relative bias. As expected from Fig. 2, this in turn has an effect on the margin of the configurations. We plot in Fig. 8 the evolution of margins (computed as $(\min_i \langle U_i, V_i \rangle - \max_{i \neq j} \langle U_i, V_j \rangle)/2)$ for different fixed relative biases and in Fig. 9 the final optimal relative biases (computed as $(\min_i \langle U_i, V_i \rangle + \max_{i \neq j} \langle U_i, V_j \rangle)/2)$.
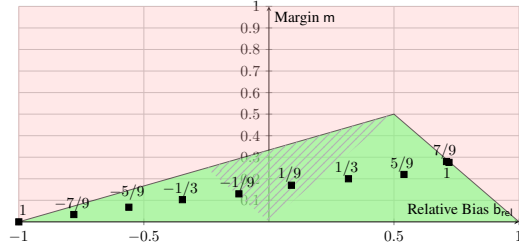
Figure 9: Achieved optimal relative bias and margin when training with a fixed relative bias. The annotations correspond to the fixed relative bias.

Locked Encoder. In particular, this gives a concrete recipe for training via the sigmoid loss with a fixed representation: one just adds a simple adapter $\mathsf{A}^\delta_{\mathsf{locked}}$ that transforms $X_i \longrightarrow (\delta X_i, \sqrt{1 - \delta^2})$ for the locked representation and $\mathsf{A}^\delta_{\mathsf{trainable}}$ that transforms $X_i \longrightarrow (\delta X_i, -\sqrt{1 - \delta^2})$ for the trainable representation. It turns out that the relative bias parametrization captures this transformation *without explicitly adding an adapter*.

Observation 1. *For any* $\{(U_i, V_i)\}_{i=1}^{N}$ *and* $\delta, \mathsf{b_{rel}}, t$, *it is the case that*

$$
\mathcal{L}^{\mathsf{RB-Sig}}(\{(\mathsf{A}^\delta_{\mathsf{lock}}(U_i), \mathsf{A}^\delta_{\mathsf{train}}(V_i)\}_{i=1}^{N}; t, \mathsf{b_{rel}}) = \mathcal{L}^{\mathsf{RB-Sig}}(\{(U_i, V_i)\}_{i=1}^{N}; t\delta^2, \frac{\mathsf{b_{rel}} + (1 - \delta)^2}{\delta^2}).
$$

As we can see in Figure 10, the models with trainable t, b (respectively $t, \mathsf{b_{rel}}$) significantly outperform the model with fixed temperature and bias. Furthermore, the convergence to zero loss is faster for $\mathcal{L}^{\mathsf{RB-Sig}}$ than $\mathcal{L}^{\mathsf{Sig}}$. Thus, we recommend synchronizing with $\mathcal{L}^{\mathsf{RB-Sig}}$ and *trainable* $t, \mathsf{b_{rel}}$.
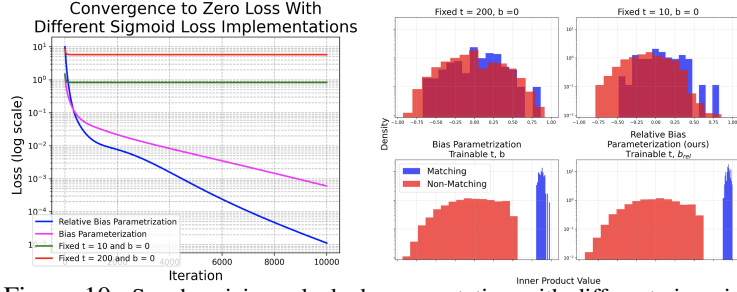

Figure 10: Synchronizing a locked representation with different sigmoid loss functions on synthetic data. On the left, we have the evolution of the loss function. On the right, we show the distributions of non-matching inner products $\langle U_i, V_j \rangle$ for $i \neq j$ in red and matching inner products $\langle U_i, V_i \rangle$ in blue for each model.

More Modalities and A New Perspective on Simplex Embeddings. Our discussion so far has been predominantly in the case of two modalities. To synchronize the representations $\{(U_i^{(1)}, \ldots, U_i^{(k)})\}_{i=1}^N$ of $k > 2$ modalities, one typically minimizes the sum of several pairwise losses [TKI20a, GENL$^+$23]. More formally, if $G = (V, E)$ is the

Figure 11: Inner product distributions between $k = 4$ modalities synchronized with different implementations of sigmoid loss. We plot the same data as in 10.

synchronization graph on vertex set $V = \{1, 2, \ldots, k\}$ the different modalities, one minimizes

$$\sum_{(j_1, j_2) \in E} \mathcal{L}^{\mathsf{RB-Sig}}(\{(U_i^{(j_1)}, U_i^{(j_2)})\}_{i=1}^N; t, \mathsf{b_{rel}}). \tag{10}$$

Common instances are when G is the complete graph and one sums over all pairwise losses [TKI20a], and when G is a star graph with one central modality [GENL$^+$23]. Since the loss function $\mathcal{L}^{\mathsf{Sig}}$ is non-negative, a configuration $\{(U_i^{(1)}, \ldots, U_i^{(k)})\}_{i=1}^N$ is *zero-loss* if and only if there exist some $\mathsf{m}, \mathsf{b_{rel}}$ such that $\{(U_i^{(j_1)}, U_i^{(j_2)})\}_{i=1}^N, \mathsf{m}, \mathsf{b_{rel}}$ is zero loss for any $(j_1, j_2) \in E$. In particular, $\{(U_i^{(1)}, \ldots, U_i^{(k)})\}_{i=1}^N$ is zero loss if there exist some $\mathsf{m}, \mathsf{b_{rel}}$ such that $\{(U_i^{(j_1)}, U_i^{(j_2)})\}_{i=1}^N, \mathsf{m}, \mathsf{b_{rel}}$ is zero loss for all $j_1 \neq j_2$. This leads us to the following construction.

Construction 2 (Construction of Constellations). *Consider any $(d - k + 1, \alpha)$-code $\{X_i\}_{i=1}^N$. Let $w_1, w_2, \ldots, w_k \in \mathbb{S}^{k-1}$ be the vertices of a regular k-simplex. Then, for any $\delta \in [0, 1)$, the following configuration is zero loss for any synchronization graph:*

$$U_i^{(j)} = (\delta X_i, \sqrt{1 - \delta^2} w_j), \qquad \mathsf{m} = \frac{\delta^2(1 - \alpha)}{2}, \qquad \mathsf{b_{rel}} = \frac{\delta^2(1 - \alpha)}{2} - \frac{1 - \delta^2}{k - 1}. \tag{11}$$

We can enforce this structure by adding an adapter which appends a modality-dependent suffix to the representation. Again the adapters can be implicitly captured by the relative bias since $\langle w_i, w_j \rangle = -\frac{1}{k-1}$ for all $i \neq j$.

Observation 2. *For any $\{(U_i^{(1)}, U_i^{(2)}, \ldots, U_i^{(k)})\}_{i=1}^N$ and $\delta, \mathsf{b_{rel}}, t,$*

$$\mathcal{L}^{\mathsf{RB-Sig}}\left(\{\mathsf{A}_1^\delta(U_i^{(1)}), \ldots, \mathsf{A}_k^\delta(U_i^{(k)})\}_{i=1}^N; t, \mathsf{b_{rel}}\right)$$

$$= \mathcal{L}^{\mathsf{RB-Sig}}\left(\{U_i^{(1)}, \ldots, U_i^{(k)}\}_{i=1}^N; t\delta^2, \mathsf{b_{rel}} + \frac{(1-\delta)^2}{k-1}\right).$$
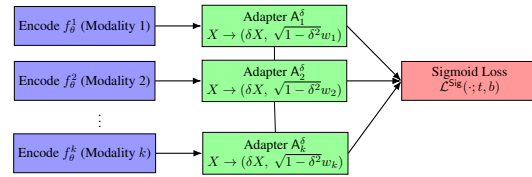

Figure 12: Adapters used to synchronize $k > 2$ modalities with sigmoid loss.

11

3.5 Ablation Studies

Training the temperature and bias is the key mechanism that drives the loss to zero for a wide range of configurations which we described as $(\mathsf{m}, \mathsf{b}_{\mathsf{rel}})$-Constellations. We compared our proposal of training $\mathcal{L}^{\mathsf{RB-Sig}}$ with trainable $\mathsf{b}_{\mathsf{rel}}, t$ parameters against several alternatives. We concretely focus on the *inner product separation condition* $\min_i \langle U_i, V_i \rangle \geq \max_{i \neq j} \langle U_i, V_j \rangle$ and corresponding margin. This is a key property of interest since, as explained, it determines the success of the model on retrieval via (approximate) nearest neighbor search. We also analyze the convergence of the loss to zero, which is an indicator for how many epochs of training a model needs till convergence.

1. Training with fixed low inverse temperature ($t \lesssim 10$) and bias as in the analysis of [LCS24] is a first natural alternative. We observed that in the contexts of synchronizing multiple embeddings (Figure 11) and synchronizing with a locked encoder (Figure 10), the resulting embeddings fail to satisfy the inner product separation condition or do so with a much smaller margin than models with trainable inverse temperature and (relative) bias.

2. Training with fixed high inverse temperature ($t \gg 10$) and bias. Any $(\mathsf{m}, \mathsf{b}_{\mathsf{rel}})$-constellation is nearly a global minimum in the regime of large t, so one may expect similar performance to the trainable inverse temperature and bias model. This approach fails in practice since it does not allow the algorithm to gradually find the synchronized representations. The embeddings discovered are not useful towards retrieval as the inner-product separation fails and the loss does not approach zero (Figures 10 and 11), even though representations with nearly-zero loss exist due to the low temperature.

3. Training with bias parameterization. Finally, we compared against the bias parameterization $\mathcal{L}^{\mathsf{Sig}}$ used in [ZMKB23b, TGW+25b]. While this model also generally led to $(\mathsf{m}, \mathsf{b}_{\mathsf{rel}})$-Constellations which can be used for perfect retrieval, we observed *slower convergence of the loss function* and *smaller margin* due to a tendency towards zero relative bias (Figures 10 and 11).

4 Limitations and Future Directions

We provide the first theoretical analysis of synchronizing representations in the practically relevant regime $d \ll N \ll 2^d$. A theoretical limitation is that while we identify global minimizers and empirically show that first-order methods such as Adam find them, we do not prove rigorous performance guarantees for first-order methods. Another theoretical limitation is that we do not fully resolve the combinatorial Problem 1, which as we point out is practically relevant for choosing the embedding dimension of encoders. Finally, we show that the parametrization of sigmoid loss with relative bias leads to more flexibility and faster convergence on synthetic data, but do not perform experiments with it on real data. We believe that all of these are exciting directions for future research.

We are not aware of any negative or direct impacts on society of our work. The work can have indirect societal impact as the findings are relevant to modern large-scale machine learning systems.

Acknowledgments

References

[BKS25] Parikshit Bansal, Ali Kavis, and Sujay Sanghavi. Understanding self-supervised learning via gaussian mixture models, 2025.

[BMS12] Vladimir Boltyanski, Horst Martini, and P.S Soltan. *Excursions into Combinatorial Geometry*. Universitext. Springer Nature, Netherlands, 2012.

[BPBDB23] Niccolò Biondi, Federico Pernici, Matteo Bruni, and Alberto Del Bimbo. Cores: Compatible representations via stationarity. *IEEE Trans. Pattern Anal. Mach. Intell.*, 45(8):9567–9582, August 2023.

[BPK⁺22] Minwoo Byeon, Beomhee Park, Haecheon Kim, Sungjun Lee, Woonhyuk Baek, and Saehoon Kim. Coyo-700m: Image-text pair dataset. https://github.com/kakaobrain/coyo-dataset, 2022.

[Car11] Constantin Carathéodory. Über den variabilitätsbereich der fourier'schen konstanten von positiven harmonischen funktionen. *Rendiconti del Circolo Matematico di Palermo (1884-1940)*, 32:193–217, 1911.

[CKNH20a] Ting Chen, Simon Kornblith, Mohammad Norouzi, and Geoffrey Hinton. A simple framework for contrastive learning of visual representations. In Hal Daumé III and Aarti Singh, editors, *Proceedings of the 37th International Conference on Machine Learning*, volume 119 of *Proceedings of Machine Learning Research*, pages 1597–1607. PMLR, 13–18 Jul 2020.

[CKNH20b] Ting Chen, Simon Kornblith, Mohammad Norouzi, and Geoffrey Hinton. A simple framework for contrastive learning of visual representations. In *Proceedings of the 37th International Conference on Machine Learning*, ICML'20. JMLR.org, 2020.

[CRL⁺20] Ching-Yao Chuang, Joshua Robinson, Yen-Chen Lin, Antonio Torralba, and Stefanie Jegelka. Debiased contrastive learning. *Advances in neural information processing systems*, 33:8765–8775, 2020.

[CSB⁺13] J.H Conway, N.J.A Sloane, E Bannai, R.E Borcherds, J Leech, S.P Norton, A.M Odlyzko, R.A Parker, L Queen, and B.B Venkov. *Sphere packings, lattices and groups*, volume 290 of *Grundlehren der mathematischen Wissenschaften*. Springer, third edition. edition, 2013.

[CSDS21] Soravit Changpinyo, Piyush Sharma, Nan Ding, and Radu Soricut. Conceptual 12m: Pushing web-scale image-text pre-training to recognize long-tail visual concepts. In *2021 IEEE/CVF Conference on Computer Vision and Pattern Recognition (CVPR)*, pages 3557–3567, 2021.

[CTM⁺21] Mathilde Caron, Hugo Touvron, Ishan Misra, Hervé Jegou, Julien Mairal, Piotr Bojanowski, and Armand Joulin. Emerging properties in self-supervised vision transformers. In *2021 IEEE/CVF International Conference on Computer Vision (ICCV)*, pages 9630–9640, 2021.

[CWC⁺23] Xi Chen, Xiao Wang, Soravit Changpinyo, AJ Piergiovanni, Piotr Padlewski, Daniel Salz, Sebastian Goodman, Adam Grycner, Basil Mustafa, Lucas Beyer, Alexander Kolesnikov, Joan Puigcerver, Nan Ding, Keran Rong, Hassan Akbari, Gaurav Mishra, Linting Xue, Ashish V Thapliyal, James Bradbury, Weicheng Kuo, Mojtaba Seyedhosseini, Chao Jia, Burcu Karagol Ayan, Carlos Riquelme Ruiz, Andreas Peter Steiner, Anelia Angelova, Xiaohua Zhai, Neil Houlsby, and Radu Soricut. PaLI: A jointly-scaled multilingual language-image model. In *The Eleventh International Conference on Learning Representations*, 2023.

[DGY⁺22] Jiankang Deng, Jia Guo, Jing Yang, Niannan Xue, Irene Kotsia, and Stefanos Zafeiriou. Arcface: Additive angular margin loss for deep face recognition. *IEEE Trans. Pattern Anal. Mach. Intell.*, 44(10.1):5962–5979, October 2022.

[DKAJ21] Karan Desai, Gaurav Kaul, Zubin Trivadi Aysola, and Justin Johnson. Redcaps: Web-curated image-text data created by the people, for the people. In *Thirty-fifth Conference on Neural Information Processing Systems Datasets and Benchmarks Track (Round 1)*, 2021.

[EANP24] Sayna Ebrahimi, Sercan O. Arik, Tejas Nama, and Tomas Pfister. Crome: Cross-modal adapters for efficient multimodal llm, 2024.

[EG24]   Anna Van Elst and Debarghya Ghoshdastidar. Tight pac-bayesian risk certificates for contrastive learning. *CoRR*, abs/2412.03486, 2024.

[EW22]   Weinan E and Stephan Wojtowytsch. On the emergence of simplex symmetry in the final and penultimate layers of neural network classifiers. In Joan Bruna, Jan Hesthaven, and Lenka Zdeborova, editors, *Proceedings of the 2nd Mathematical and Scientific Machine Learning Conference*, volume 145 of *Proceedings of Machine Learning Research*, pages 270–290. PMLR, 16–19 Aug 2022.

[FMF25]   Abrar Fahim, Alex Murphy, and Alona Fyshe. It's not a modality gap: Characterizing and addressing the contrastive gap, 2025.

[GENL+23] Rohit Girdhar, Alaaeldin El-Nouby, Zhuang Liu, Mannat Singh, Kalyan Vasudev Alwala, Armand Joulin, and Ishan Misra. Imagebind one embedding space to bind them all. In *2023 IEEE/CVF Conference on Computer Vision and Pattern Recognition (CVPR)*, pages 15180–15190, 2023.

[GGZ+24]   Peng Gao, Shijie Geng, Renrui Zhang, Teli Ma, Rongyao Fang, Yongfeng Zhang, Hongsheng Li, and Yu Qiao. Clip-adapter: Better vision-language models with feature adapters. *International journal of computer vision*, 132(2):581–595, 2024.

[GRL+24]   Sharut Gupta, Joshua Robinson, Derek Lim, Soledad Villar, and Stefanie Jegelka. Structuring representation geometry with rotationally equivariant contrastive learning. In *The Twelfth International Conference on Learning Representations*, 2024.

[GS25]   Nikolaos Giakoumoglou and Tania Stathaki. Discriminative and consistent representation distillation, 2025.

[GSK18]   Spyros Gidaris, Praveer Singh, and Nikos Komodakis. Unsupervised representation learning by predicting image rotations, 2018.

[HCWI24]   Minyoung Huh, Brian Cheung, Tongzhou Wang, and Phillip Isola. Position: The platonic representation hypothesis. In Ruslan Salakhutdinov, Zico Kolter, Katherine Heller, Adrian Weller, Nuria Oliver, Jonathan Scarlett, and Felix Berkenkamp, editors, *Proceedings of the 41st International Conference on Machine Learning*, volume 235 of *Proceedings of Machine Learning Research*, pages 20617–20642. PMLR, 21–27 Jul 2024.

[Hel23]   Ed. Helly. Über mengen konvexer körper mit gemeinschaftlichen punkte. *Jahresbericht der Deutschen Mathematiker-Vereinigung*, 32:175–176, 1923.

[HFLM+19] R Devon Hjelm, Alex Fedorov, Samuel Lavoie-Marchildon, Karan Grewal, Phil Bachman, Adam Trischler, and Yoshua Bengio. Learning deep representations by mutual information estimation and maximization. In *International Conference on Learning Representations*, 2019.

[HFW+20]   Kaiming He, Haoqi Fan, Yuxin Wu, Saining Xie, and Ross Girshick. Momentum contrast for unsupervised visual representation learning. In *2020 IEEE/CVF Conference on Computer Vision and Pattern Recognition (CVPR)*, pages 9726–9735, 2020.

[HGW+22]   Xiaowei Hu, Zhe Gan, Jianfeng Wang, Zhengyuan Yang, Zicheng Liu, Yumao Lu, and Lijuan Wang. Scaling up vision-language pretraining for image captioning. In *2022 IEEE/CVF Conference on Computer Vision and Pattern Recognition (CVPR)*, pages 17959–17968, 2022.

[JFF+23]   Florian Jaeckle, Fartash Faghri, Ali Farhadi, Oncel Tuzel, and Hadi Pouransari. Fastfill: Efficient compatible model update. In *The Eleventh International Conference on Learning Representations*, 2023.

[JYX+21]   Chao Jia, Yinfei Yang, Ye Xia, Yi-Ting Chen, Zarana Parekh, Hieu Pham, Quoc Le, Yun-Hsuan Sung, Zhen Li, and Tom Duerig. Scaling up visual and vision-language representation learning with noisy text supervision. In Marina Meila and Tong Zhang, editors, *Proceedings of the 38th International Conference on Machine Learning*, volume 139 of *Proceedings of Machine Learning Research*, pages 4904–4916. PMLR, 18–24 Jul 2021.

[KB15]   Diederik P. Kingma and Jimmy Ba. Adam: A method for stochastic optimization. In Yoshua Bengio and Yann LeCun, editors, *3rd International Conference on Learning Representations, ICLR 2015, San Diego, CA, USA, May 7-9, 2015, Conference Track Proceedings*, 2015.

[KZ20]   Omar Khattab and Matei Zaharia. Colbert: Efficient and effective passage search via contextualized late interaction over bert. In *Proceedings of the 43rd International ACM SIGIR Conference on Research and Development in Information Retrieval*, SIGIR '20, page 39–48, New York, NY, USA, 2020. Association for Computing Machinery.

[LCS24]   Chungpa Lee, Joonhwan Chang, and Jy-yong Sohn. Analysis of using sigmoid loss for contrastive learning. In Sanjoy Dasgupta, Stephan Mandt, and Yingzhen Li, editors, *Proceedings of The 27th International Conference on Artificial Intelligence and Statistics*, volume 238 of *Proceedings of Machine Learning Research*, pages 1747–1755. PMLR, 02–04 May 2024.

[LHY+24]   Haoyu Lu, Yuqi Huo, Guoxing Yang, Zhiwu Lu, Wei Zhan, Masayoshi Tomizuka, and Mingyu Ding. Uniadapter: Unified parameter-efficient transfer learning for cross-modal modeling. In *The Twelfth International Conference on Learning Representations*, 2024.

[LLSH23]   Junnan Li, Dongxu Li, Silvio Savarese, and Steven Hoi. Blip-2: bootstrapping language-image pre-training with frozen image encoders and large language models. In *Proceedings of the 40th International Conference on Machine Learning*, ICML'23. JMLR.org, 2023.

[LLXH22]   Junnan Li, Dongxu Li, Caiming Xiong, and Steven Hoi. BLIP: Bootstrapping language-image pre-training for unified vision-language understanding and generation. In Kamalika Chaudhuri, Stefanie Jegelka, Le Song, Csaba Szepesvari, Gang Niu, and Sivan Sabato, editors, *Proceedings of the 39th International Conference on Machine Learning*, volume 162 of *Proceedings of Machine Learning Research*, pages 12888–12900. PMLR, 17–23 Jul 2022.

[LM25]   Licong Lin and Song Mei. A statistical theory of contrastive learning via approximate sufficient statistics, 2025.

[LS22]   Jianfeng Lu and Stefan Steinerberger. Neural collapse under cross-entropy loss. *Applied and Computational Harmonic Analysis*, 59:224–241, 2022. Special Issue on Harmonic Analysis and Machine Learning.

[LWY+17]   Weiyang Liu, Yandong Wen, Zhiding Yu, Ming Li, Bhiksha Raj, and Le Song. Sphereface: Deep hypersphere embedding for face recognition. In *2017 IEEE Conference on Computer Vision and Pattern Recognition (CVPR)*, pages 6738–6746, 2017.

[LWYY16]   Weiyang Liu, Yandong Wen, Zhiding Yu, and Meng Yang. Large-margin softmax loss for convolutional neural networks. In *Proceedings of the 33rd International Conference on International Conference on Machine Learning - Volume 48*, ICML'16, page 507–516. JMLR.org, 2016.

[LXGY23]   Hongye Liu, Xianhai Xie, Yang Gao, and Zhou Yu. Parameter-efficient transfer learning for audio-visual-language tasks. In *Proceedings of the 31st ACM International Conference on Multimedia*, MM '23, page 387–396, New York, NY, USA, 2023. Association for Computing Machinery.

[LZK+22]   Weixin Liang, Yuhui Zhang, Yongchan Kwon, Serena Yeung, and James Zou. Mind the gap: Understanding the modality gap in multi-modal contrastive representation learning. In Alice H. Oh, Alekh Agarwal, Danielle Belgrave, and Kyunghyun Cho, editors, *Advances in Neural Information Processing Systems*, 2022.

[LZS+23]   Yiwei Lu, Guojun Zhang, Sun Sun, Hongyu Guo, and Yaoliang Yu. f-MICL: Understanding and generalizing infoNCE-based contrastive learning. *Transactions on Machine Learning Research*, 2023.

[MCCD13] Tomas Mikolov, Kai Chen, Greg Corrado, and Jeffrey Dean. Efficient estimation of word representations in vector space, 2013.

[Min10] H. (Hermann) Minkowski. *Geometrie der Zahlen*. Teubner, Leipzig, 1910.

[MT21] Craig Macdonald and Nicola Tonellotto. On approximate nearest neighbour selection for multi-stage dense retrieval. In *Proceedings of the 30th ACM International Conference on Information & Knowledge Management*, CIKM '21, page 3318–3322, New York, NY, USA, 2021. Association for Computing Machinery.

[NF16] Mehdi Noroozi and Paolo Favaro. Unsupervised learning of visual representations by solving jigsaw puzzles. In Bastian Leibe, Jiri Matas, Nicu Sebe, and Max Welling, editors, *Computer Vision – ECCV 2016*, pages 69–84, Cham, 2016. Springer International Publishing.

[OLCM25] Kazusato Oko, Licong Lin, Yuhang Cai, and Song Mei. A statistical theory of contrastive pre-training and multimodal generative ai, 2025.

[PCV24] Kiho Park, Yo Joong Choe, and Victor Veitch. The linear representation hypothesis and the geometry of large language models. In *Proceedings of the 41st International Conference on Machine Learning*, ICML'24. JMLR.org, 2024.

[PHD20] Vardan Papyan, X. Y. Han, and David L. Donoho. Prevalence of neural collapse during the terminal phase of deep learning training. *Proceedings of the National Academy of Sciences*, 117(40):24652–24663, 2020.

[PVZ15] Omkar M. Parkhi, Andrea Vedaldi, and Andrew Zisserman. Deep face recognition. In *British Machine Vision Conference*, 2015.

[Ran55] R. A. Rankin. The closest packing of spherical caps in n dimensions. *Proceedings of the Glasgow Mathematical Association*, 2(3):139–144, 1955.

[RAVF+22] Vivek Ramanujan, Pavan Kumar Anasosalu Vasu, Ali Farhadi, Oncel Tuzel, and Hadi Pouransari. Forward compatible training for large-scale embedding retrieval systems. In *2022 IEEE/CVF Conference on Computer Vision and Pattern Recognition (CVPR)*, pages 19364–19373, 2022.

[RCSJ21] Joshua David Robinson, Ching-Yao Chuang, Suvrit Sra, and Stefanie Jegelka. Contrastive learning with hard negative samples. In *International Conference on Learning Representations*, 2021.

[RKH+21] Alec Radford, Jong Wook Kim, Chris Hallacy, Aditya Ramesh, Gabriel Goh, Sandhini Agarwal, Girish Sastry, Amanda Askell, Pamela Mishkin, Jack Clark, Gretchen Krueger, and Ilya Sutskever. Learning transferable visual models from natural language supervision. In Marina Meila and Tong Zhang, editors, *Proceedings of the 38th International Conference on Machine Learning*, volume 139 of *Proceedings of Machine Learning Research*, pages 8748–8763. PMLR, 18–24 Jul 2021.

[RNP+22] Elan Rosenfeld, Preetum Nakkiran, Hadi Pouransari, Oncel Tuzel, and Fartash Faghri. APE: Aligning pretrained encoders to quickly learn aligned multimodal representations. In *Has it Trained Yet? NeurIPS 2022 Workshop*, 2022.

[SBV+22] Christoph Schuhmann, Romain Beaumont, Richard Vencu, Cade W Gordon, Ross Wightman, Mehdi Cherti, Theo Coombes, Aarush Katta, Clayton Mullis, Mitchell Wortsman, Patrick Schramowski, Srivatsa R Kundurthy, Katherine Crowson, Ludwig Schmidt, Robert Kaczmarczyk, and Jenia Jitsev. LAION-5b: An open large-scale dataset for training next generation image-text models. In *Thirty-sixth Conference on Neural Information Processing Systems Datasets and Benchmarks Track*, 2022.

[Sha59] Claude E. Shannon. Probability of error for optimal codes in a gaussian channel. *Bell System Technical Journal*, 38(3):611–656, 1959.

[SKP15] Florian Schroff, Dmitry Kalenichenko, and James Philbin. Facenet: A unified embedding for face recognition and clustering. In *Proceedings of the IEEE Conference on Computer Vision and Pattern Recognition (CVPR)*, June 2015.

[SPA+19] Nikunj Saunshi, Orestis Plevrakis, Sanjeev Arora, Mikhail Khodak, and Hrishikesh Khandeparkar. A theoretical analysis of contrastive unsupervised representation learning. In Kamalika Chaudhuri and Ruslan Salakhutdinov, editors, *Proceedings of the 36th International Conference on Machine Learning, ICML 2019, 9-15 June 2019, Long Beach, California, USA*, volume 97 of *Proceedings of Machine Learning Research*, pages 5628–5637. PMLR, 2019.

[SRC+21] Krishna Srinivasan, Karthik Raman, Jiecao Chen, Michael Bendersky, and Marc Najork. Wit: Wikipedia-based image text dataset for multimodal multilingual machine learning. In *Proceedings of the 44th International ACM SIGIR Conference on Research and Development in Information Retrieval*, SIGIR '21, page 2443–2449, New York, NY, USA, 2021. Association for Computing Machinery.

[Ste13] Ernst Steinitz. Bedingt konvergente reihen und konvexe systeme. *Journal für die reine und angewandte Mathematik*, 143:128–176, 1913.

[SXXS20] Yantao Shen, Yuanjun Xiong, Wei Xia, and Stefano Soatto. Towards backward-compatible representation learning. *2020 IEEE/CVF Conference on Computer Vision and Pattern Recognition (CVPR)*, pages 6367–6376, 2020.

[TCM+24] Adly Templeton, Tom Conerly, Jonathan Marcus, Jack Lindsey, Trenton Bricken, Brian Chen, Adam Pearce, Craig Citro, Emmanuel Ameisen, Andy Jones, Hoagy Cunningham, Nicholas L Turner, Callum McDougall, Monte MacDiarmid, C. Daniel Freeman, Theodore R. Sumers, Edward Rees, Joshua Batson, Adam Jermyn, Shan Carter, Chris Olah, and Tom Henighan. Scaling monosemanticity: Extracting interpretable features from claude 3 sonnet. *Transformer Circuits Thread*, 2024.

[TGW+25a] Michael Tschannen, Alexey Gritsenko, Xiao Wang, Muhammad Ferjad Naeem, Ibrahim Alabdulmohsin, Nikhil Parthasarathy, Talfan Evans, Lucas Beyer, Ye Xia, Basil Mustafa, et al. Siglip 2: Multilingual vision-language encoders with improved semantic understanding, localization, and dense features. *arXiv preprint arXiv:2502.14786*, 2025.

[TGW+25b] Michael Tschannen, Alexey Gritsenko, Xiao Wang, Muhammad Ferjad Naeem, Ibrahim Alabdulmohsin, Nikhil Parthasarathy, Talfan Evans, Lucas Beyer, Ye Xia, Basil Mustafa, Olivier Hénaff, Jeremiah Harmsen, Andreas Steiner, and Xiaohua Zhai. Siglip 2: Multilingual vision-language encoders with improved semantic understanding, localization, and dense features, 2025.

[TKF+25] Gemma Team, Aishwarya Kamath, Johan Ferret, Shreya Pathak, Nino Vieillard, Ramona Merhej, Sarah Perrin, Tatiana Matejovicova, Alexandre Ramé, Morgane Rivière, Louis Rouillard, Thomas Mesnard, Geoffrey Cideron, Jean bastien Grill, Sabela Ramos, Edouard Yvinec, Michelle Casbon, Etienne Pot, Ivo Penchev, Gaël Liu, Francesco Visin, Kathleen Kenealy, Lucas Beyer, Xiaohai Zhai, Anton Tsitsulin, Robert Busa-Fekete, Alex Feng, Noveen Sachdeva, Benjamin Coleman, Yi Gao, Basil Mustafa, Iain Barr, Emilio Parisotto, David Tian, Matan Eyal, Colin Cherry, Jan-Thorsten Peter, Danila Sinopalnikov, Surya Bhupatiraju, Rishabh Agarwal, Mehran Kazemi, Dan Malkin, Ravin Kumar, David Vilar, Idan Brusilovsky, Jiaming Luo, Andreas Steiner, Abe Friesen, Abhanshu Sharma, Abheesht Sharma, Adi Mayrav Gilady, Adrian Goedeckemeyer, Alaa Saade, Alex Feng, Alexander Kolesnikov, Alexei Bendebury, Alvin Abdagic, Amit Vadi, András György, André Susano Pinto, Anil Das, Ankur Bapna, Antoine Miech, Antoine Yang, Antonia Paterson, Ashish Shenoy, Ayan Chakrabarti, Bilal Piot, Bo Wu, Bobak Shahriari, Bryce Petrini, Charlie Chen, Charline Le Lan, Christopher A. Choquette-Choo, CJ Carey, Cormac Brick, Daniel Deutsch, Danielle Eisenbud, Dee Cattle, Derek Cheng, Dimitris Paparas, Divyashree Shivakumar Sreepathihalli, Doug Reid, Dustin Tran, Dustin Zelle, Eric Noland, Erwin Huizenga, Eugene Kharitonov, Frederick Liu, Gagik Amirkhanyan, Glenn Cameron, Hadi Hashemi,

Hanna Klimczak-Plucińska, Harman Singh, Harsh Mehta, Harshal Tushar Lehri, Hussein Hazimeh, Ian Ballantyne, Idan Szpektor, Ivan Nardini, Jean Pouget-Abadie, Jetha Chan, Joe Stanton, John Wieting, Jonathan Lai, Jordi Orbay, Joseph Fernandez, Josh Newlan, Ju yeong Ji, Jyotinder Singh, Kat Black, Kathy Yu, Kevin Hui, Kiran Vodrahalli, Klaus Greff, Linhai Qiu, Marcella Valentine, Marina Coelho, Marvin Ritter, Matt Hoffman, Matthew Watson, Mayank Chaturvedi, Michael Moynihan, Min Ma, Nabila Babar, Natasha Noy, Nathan Byrd, Nick Roy, Nikola Momchev, Nilay Chauhan, Noveen Sachdeva, Oskar Bunyan, Pankil Botarda, Paul Caron, Paul Kishan Rubenstein, Phil Culliton, Philipp Schmid, Pier Giuseppe Sessa, Pingmei Xu, Piotr Stanczyk, Pouya Tafti, Rakesh Shivanna, Renjie Wu, Renke Pan, Reza Rokni, Rob Willoughby, Rohith Vallu, Ryan Mullins, Sammy Jerome, Sara Smoot, Sertan Girgin, Shariq Iqbal, Shashir Reddy, Shruti Sheth, Siim Põder, Sijal Bhatnagar, Sindhu Raghuram Panyam, Sivan Eiger, Susan Zhang, Tianqi Liu, Trevor Yacovone, Tyler Liechty, Uday Kalra, Utku Evci, Vedant Misra, Vincent Roseberry, Vlad Feinberg, Vlad Kolesnikov, Woohyun Han, Woosuk Kwon, Xi Chen, Yinlam Chow, Yuvein Zhu, Zichuan Wei, Zoltan Egyed, Victor Cotruta, Minh Giang, Phoebe Kirk, Anand Rao, Kat Black, Nabila Babar, Jessica Lo, Erica Moreira, Luiz Gustavo Martins, Omar Sanseviero, Lucas Gonzalez, Zach Gleicher, Tris Warkentin, Vahab Mirrokni, Evan Senter, Eli Collins, Joelle Barral, Zoubin Ghahramani, Raia Hadsell, Yossi Matias, D. Sculley, Slav Petrov, Noah Fiedel, Noam Shazeer, Oriol Vinyals, Jeff Dean, Demis Hassabis, Koray Kavukcuoglu, Clement Farabet, Elena Buchatskaya, Jean-Baptiste Alayrac, Rohan Anil, Dmitry, Lepikhin, Sebastian Borgeaud, Olivier Bachem, Armand Joulin, Alek Andreev, Cassidy Hardin, Robert Dadashi, and Léonard Hussenot. Gemma 3 technical report, 2025.

[TKI20a]   Yonglong Tian, Dilip Krishnan, and Phillip Isola. Contrastive multiview coding. In Andrea Vedaldi, Horst Bischof, Thomas Brox, and Jan-Michael Frahm, editors, *Computer Vision – ECCV 2020*, pages 776–794, Cham, 2020. Springer International Publishing.

[TKI20b]   Yonglong Tian, Dilip Krishnan, and Phillip Isola. Contrastive representation distillation. In *International Conference on Learning Representations*, 2020.

[vdOLV19]   Aaron van den Oord, Yazhe Li, and Oriol Vinyals. Representation learning with contrastive predictive coding, 2019.

[WBNL25]   Orion Weller, Michael Boratko, Iftekhar Naim, and Jinhyuk Lee. On the theoretical limitations of embedding-based retrieval. *arXiv preprint arXiv:2508.21038*, 2025.

[WI20]   Tongzhou Wang and Phillip Isola. Understanding contrastive representation learning through alignment and uniformity on the hypersphere. In *Proceedings of the 37th International Conference on Machine Learning*, ICML'20. JMLR.org, 2020.

[WXCY17]   Feng Wang, Xiang Xiang, Jian Cheng, and Alan Loddon Yuille. Normface: L2 hypersphere embedding for face verification. In *Proceedings of the 25th ACM International Conference on Multimedia*, MM '17, page 1041–1049, New York, NY, USA, 2017. Association for Computing Machinery.

[WYH+22]   Jianfeng Wang, Zhengyuan Yang, Xiaowei Hu, Linjie Li, Kevin Lin, Zhe Gan, Zicheng Liu, Ce Liu, and Lijuan Wang. GIT: A generative image-to-text transformer for vision and language. *CoRR*, abs/2205.14100, 2022.

[Wyn68]   A. D. Wyner. Communication of analog data from a gaussian source over a noisy channel. *Bell System Technical Journal*, 47(5):801–812, 1968.

[XXL+21]   Lee Xiong, Chenyan Xiong, Ye Li, Kwok-Fung Tang, Jialin Liu, Paul N. Bennett, Junaid Ahmed, and Arnold Overwijk. Approximate nearest neighbor negative contrastive learning for dense text retrieval. In *International Conference on Learning Representations*, 2021.

[YZWX24]   Lingxiao Yang, Ru-Yuan Zhang, Yanchen Wang, and Xiaohua Xie. Mma: Multi-modal adapter for vision-language models. In *Proceedings of the IEEE/CVF Conference on Computer Vision and Pattern Recognition (CVPR)*, pages 23826–23837, June 2024.

[ZIE⁺16] Richard Zhang, Phillip Isola, Alexei A. Efros, Nicu Sebe, Jiri Matas, Max Welling, and Bastian Leibe. Colorful image colorization. In *Computer Vision - ECCV 2016*, volume 9907 of *Lecture Notes in Computer Science*, pages 649–666. Springer International Publishing AG, Switzerland, 2016.

[ZMKB23a] Xiaohua Zhai, Basil Mustafa, Alexander Kolesnikov, and Lucas Beyer. Siglip demo experiments by, 2023.

[ZMKB23b] Xiaohua Zhai, Basil Mustafa, Alexander Kolesnikov, and Lucas Beyer. Sigmoid loss for language image pre-training. In *2023 IEEE/CVF International Conference on Computer Vision (ICCV)*, pages 11941–11952, 2023.

[ZWM⁺22] Xiaohua Zhai, Xiao Wang, Basil Mustafa, Andreas Steiner, Daniel Keysers, Alexander Kolesnikov, and Lucas Beyer. Lit: Zero-shot transfer with locked-image text tuning. In *2022 IEEE/CVF Conference on Computer Vision and Pattern Recognition (CVPR)*, pages 18102–18112, 2022.

[ZZF⁺22] Renrui Zhang, Wei Zhang, Rongyao Fang, Peng Gao, Kunchang Li, Jifeng Dai, Yu Qiao, and Hongsheng Li. Tip-adapter: Training-free adaption of clip for few-shot classification. In *Computer Vision – ECCV 2022: 17th European Conference, Tel Aviv, Israel, October 23–27, 2022, Proceedings, Part XXXV*, page 493–510, Berlin, Heidelberg, 2022. Springer-Verlag.

A Omitted Proofs From Section 3.1

A.1 Global Minimizers of The Sigmoid Loss are $(\mathsf{m}, \mathsf{b}_{\mathsf{rel}})$-Constellations

We will repeatedly use the following fact which follows from $\log(1 + \exp(\kappa)) \geq 0$ for any $\kappa \in \mathbb{R}$.

Observation 3. *For any $\{(U_i, V_i)\}_{i=1}^N$ and t, b, it holds that*

$$\max\left(\max_i \log\left(1 + \exp(-t\langle U_i, V_i\rangle + b)\right), \max_{i \neq j} \log\left(1 + \exp(t\langle U_i, V_j\rangle - b)\right)\right) \tag{12}$$

$$\leq \mathcal{L}^{\mathsf{Sig}}(\{U_i\}_{i=1}^N, \{V_i\}_{i=1}^N; t, b)$$

$$\leq N^2 \times \max\left(\max_i \log\left(1 + \exp(-t\langle U_i, V_i\rangle + b)\right), \max_{i \neq j} \log\left(1 + \exp(t\langle U_i, V_j\rangle - b)\right)\right). \tag{13}$$

Proof of Theorem 3.1. Suppose that $\lim_{s \longrightarrow +\infty} \mathcal{L}^{\mathsf{Sig}}(\{U_i^{(s)}\}_{i=1}^N, \{V_i^{(s)}\}_{i=1}^N; t^{(s)}, b^{(s)}) = 0$ indeed holds. By, (12), this means that

$$\lim_{s \longrightarrow +\infty} \log\left(1 + \exp(-t^{(s)}\langle U_i^{(s)}, V_i^{(s)}\rangle + b^{(s)})\right) = 0 \qquad \forall i,$$

$$\lim_{s \longrightarrow +\infty} \log\left(1 + \exp(t^{(s)}\langle U_i^{(s)}, V_j^{(s)}\rangle - b^{(s)})\right) = 0 \qquad \forall i \neq j.$$

Equivalently,

$$\lim_{s \longrightarrow +\infty} -t^{(s)}\langle U_i^{(s)}, V_i^{(s)}\rangle + b^{(s)} = -\infty \qquad \forall i,$$

$$\lim_{s \longrightarrow +\infty} t^{(s)}\langle U_i^{(s)}, V_j^{(s)}\rangle - b^{(s)} = -\infty \qquad \forall i \neq j.$$

Equivalently,

$$\lim_{s \longrightarrow +\infty} t^{(s)}\left(\langle U_i^{(s)}, V_i^{(s)}\rangle - \frac{b^{(s)}}{t^{(s)}}\right) = +\infty \qquad \forall i,$$

$$\lim_{s \longrightarrow +\infty} t^{(s)}\left(\langle U_i^{(s)}, V_j^{(s)}\rangle - \frac{b^{(s)}}{t^{(s)}}\right) = -\infty \qquad \forall i \neq j.$$

In particular, as $t^{(s)} > 0$ always, this means that for all large enough s, the quantity $\mathsf{b}_{\mathsf{rel}}^{(s)} := \frac{b^{(s)}}{t^{(s)}}$ satisfies that

$$\langle U_i^{(s)}, V_i^{(s)}\rangle - \mathsf{b}_{\mathsf{rel}}^{(s)} \geq 0 \qquad \forall i, \tag{14}$$

$$\langle U_i^{(s)}, V_j^{(s)}\rangle - \mathsf{b}_{\mathsf{rel}}^{(s)} \leq 0 \qquad \forall i \neq j. \tag{15}$$

However, as all $U_i^{(s)}, V_i^{(s)}$ are unit vectors, $\langle U_i^{(s)}, V_i^{(s)}\rangle \leq 1, \langle U_i^{(s)}, V_j^{(s)}\rangle \geq -1$ holds for any i, j, s. Hence, for all large enough s, (14) and (15) imply that

$$-1 \leq \mathsf{b}_{\mathsf{rel}}^{(s)} \leq 1.$$

Now, observe that $\{U_1^{(s)}, U_2^{(s)}, \ldots, U_N^{(s)}, V_1^{(s)}, V_2^{(s)}, \ldots, V_N^{(s)}, \mathsf{b}_{\mathsf{rel}}^{(s)}\} \in (\mathbb{S}^{d-1})^{\otimes 2N} \times [-1, 1]$. As $(\mathbb{S}^{d-1})^{\otimes 2N} \times [-1, 1]$ is a compact set, $\{U_1^{(s)}, U_2^{(s)}, \ldots, U_N^{(s)}, V_1^{(s)}, V_2^{(s)}, \ldots, V_N^{(s)}, \mathsf{b}_{\mathsf{rel}}^{(s)}\}_{s=1}^{+\infty}$ has a convergent subsequence. Suppose that it converges to $\{U_1, U_2, \ldots, U_N, V_1, V_2, \ldots, V_N, \mathsf{b}_{\mathsf{rel}}\}$. By (14) and (15), we have that

$$\langle U_i, V_i\rangle - \mathsf{b}_{\mathsf{rel}} \geq 0 \qquad \forall i, \tag{16}$$

$$\langle U_i, V_j\rangle - \mathsf{b}_{\mathsf{rel}} \leq 0 \qquad \forall i \neq j. \tag{17}$$

Setting

$$\mathsf{m} = \min\left(\min_i \langle U_i, V_i\rangle - \mathsf{b}_{\mathsf{rel}}, \min_{i \neq j} \mathsf{b}_{\mathsf{rel}} - \langle U_i, V_j\rangle\right)$$

gives the desired result. $\qquad \square$

Proof of Theorem 3.2. Suppose that $\{(U_i, V_i)\}_{i=1}^N$ are a $(\mathsf{m}, \mathsf{b_{rel}})$-Constellation with some $\mathsf{m} > 0$. Then, for any t, it holds that

$$t(\langle U_i, V_i\rangle - \mathsf{b_{rel}}) \geq \mathsf{m} \times t \qquad \forall i, \tag{18}$$
$$t(\langle U_i, V_j\rangle - \mathsf{b_{rel}}) \leq -\mathsf{m} \times t \qquad \forall i \neq j. \tag{19}$$

In particular, by Observation (13), it follows that

$$\mathcal{L}^{\mathsf{Sig}}(\{U_i\}_{i=1}^N, \{V_i\}_{i=1}^N; t, t\mathsf{b_{rel}})$$
$$\leq N^2 \times \log\left(1 + \exp(-\mathsf{m} \times t)\right)$$
$$\leq N^2 \exp(-\mathsf{m} \times t) = \exp(-\mathsf{m} \times t + 2\log N/t) = \exp(-\mathsf{m} \times t + o(t))$$

which proves the convergence to zero. Choosing $(\mathsf{m}^*, \mathsf{b_{rel}^*})$ in this argument, where

$$\mathsf{m}^* := \frac{1}{2}(\min_i \langle U_i, V_i\rangle - \max_{i \neq j}\langle U_i, V_j\rangle) > \frac{1}{2}((\mathsf{m} + \mathsf{b_{rel}}) - (-\mathsf{m} + \mathsf{b_{rel}})) = \mathsf{m} > 0,$$

$$\mathsf{b_{rel}^*} := \frac{1}{2}(\min_i \langle U_i, V_i\rangle + \max_{i \neq j}\langle U_i, V_j\rangle),$$

also proves that $\inf_b \mathcal{L}^{\mathsf{Sig}}(\{U_i\}_{i=1}^N, \{V_i\}_{i=1}^N; t, b) \leq e^{-t\mathsf{m}^* + o(t)}$.

All that is left to show is that

$$\inf_b \mathcal{L}^{\mathsf{Sig}}(\{U_i\}_{i=1}^N, \{V_i\}_{i=1}^N; t, b) \geq e^{-t\mathsf{m}^* + o(t)}.$$

Equivalently, we can show that $\inf_b \mathcal{L}^{\mathsf{Sig}}(\{U_i\}_{i=1}^N, \{V_i\}_{i=1}^N; t, b) \geq \log\left(1 + e^{-t\mathsf{m}^* + o(t)}\right)$ since $\log(1 + \gamma) = \gamma + o(\gamma)$ as $\gamma \longrightarrow 0$. However, by (12), for the last inequality, it is enough to show that

$$\max\left(\max_i\left(-t\langle U_i, V_i\rangle + b\right)\right), \max_{i \neq j}\left(t\langle U_i, V_j\rangle - b\right)\right) \geq -t \times \mathsf{m}^*.$$

Equivalently

$$\min\left(\min_i\left(\langle U_i, V_i\rangle - \frac{b}{t}\right)\right), \min_{i \neq j}\left(-t\langle U_i, V_j\rangle + \frac{b}{t}\right)\right) \leq \mathsf{m}^*.$$

Suppose, for the sake of contradiction, that for some b, t, we have that

$$\min\left(\min_i\left(\langle U_i, V_i\rangle - \frac{b}{t}\right)\right), \min_{i \neq j}\left(-t\langle U_i, V_j\rangle + \frac{b}{t}\right)\right) = \mathsf{m}' > \mathsf{m}^*.$$

Then,

$$\min_i \langle U_i, V_i\rangle - \max_{i \neq j}\langle U_i, V_j\rangle \geq \frac{b}{t} + \mathsf{m}' - (\frac{b}{t} - \mathsf{m}') = 2\mathsf{m}' > 2\mathsf{m}^*,$$

which is a contradiction with the definition of m^*. $\qquad\square$

A.2 Robustness of Nearest-Neighbor Retrieval: Proof of Proposition 1

Suppose that

$$\mathbb{E}_{(a_j)_{j=1}^B \sim [N]^{\times k}}\left[\sum_{j=1}^B \log\left(1 + \exp(-t\langle U_{a_j}, V_{a_j}\rangle + b)\right)\right.$$
$$\left. + \sum_{i \neq j}\log\left(1 + \exp(t\langle U_{a_i}, V_{a_j}\rangle - b)\right)\right] \leq \xi\log 2.$$

holds. Again, as the function $x \longrightarrow \log(1 + e^x)$ is non-negative, this implies that for some $0 \leq x \leq \xi$,

$$x\log 2 = \mathbb{E}_{(a_j)_{j=1}^B \sim [N]^{\times k}}\left[\sum_{j=1}^B \log\left(1 + \exp(-t\langle U_{a_j}, V_{a_j}\rangle + b)\right)\right]$$
$$= B \times \mathbb{E}_{j \sim \mathsf{unif}([N])}\log\left(1 + \exp(-t\langle U_j, V_j\rangle + b)\right).$$

However, whenever $t\langle U_j, V_j \rangle - b \leq 0$, then $\log\left(1 + \exp(-t\langle U_j, V_j \rangle + b)\right) \geq \log 2$. By Markov's inequality, it follows that

$$\mathop{\mathbb{P}}_{j \sim \mathsf{unif}([N])}[t\langle U_j, V_j \rangle - b \leq 0] \leq \frac{x}{B}.$$

Hence, for all but at most a $\frac{x}{B}$ fraction of the data indices j, it follows that $\langle U_j, V_j \rangle > b/t$.

In the exact same way, for some $y \geq 0$ such that $x + y \leq \xi$. it follows that

$$\mathop{\mathbb{P}}_{i,j \sim [N]^{\times 2}}[t\langle U_j, V_j \rangle - b \geq 0] \leq \frac{y}{B(B-1)}.$$

Note that for every fixed i, if $\mathbb{P}_{j \sim \mathsf{unif}([N])|_{j \neq i}}[t\langle U_j, V_j \rangle - b > 0] > 0$, then $\mathbb{P}_{j \sim \mathsf{unif}([N])|_{j \neq i}}[t\langle U_j, V_j \rangle - b > 0] \geq 1/(N-1)$. Hence, one can similarly argue that for all but at most a $\frac{y(N-1)}{B(B-1)}$ fraction of the data indices i, it follows that $\langle U_i, V_j \rangle < b/t$ for all j. Thus, for at least a

$$1 - \frac{x}{B} - \frac{y(N-1)}{B(B-1)}$$

fraction of the indices i, it follows that for any $j \neq i$,

$$\langle U_i, V_i \rangle > b/t > \langle U_i, V_j \rangle.$$

Clearly, for these indices, nearest neighbor search succeeds. Optimizing over $0 \leq x, 0 \leq y, x + y \leq \xi$, we reach the conclusion.

A.3 Triplet Loss

In the context of synchronizing embeddings, the triplet loss function [SKP15] with hyperparameter margin α takes form

$$\mathcal{L}^{\mathsf{Triplet}}(\{(U_i, V_i)\}_{i=1}^N; \alpha) = \sum_{i \neq j} \max(\|U_i - V_i\|_2^2 - \|U_i - V_j\|_2^2 + \alpha, 0). \tag{20}$$

Observation 4. *Suppose that* $\{(U_i, V_i)\}_{i=1}^N$ *is a* $(\mathsf{m}, \mathsf{b_{rel}})$-*Constellation. Then, for any* $\alpha \leq 4\mathsf{m}$, *it is also the case that*

$$\mathcal{L}^{\mathsf{Triplet}}(\{(U_i, V_i)\}_{i=1}^N; \alpha) = 0.$$

Proof. Suppose that $\{(U_i, V_i)\}_{i=1}^N$ is a $(\mathsf{m}, \mathsf{b_{rel}})$-Constellation. Then, for any $i, \neq j$, we have that

$$\begin{aligned}
&\|U_i - V_i\|_2^2 - \|U_i - V_j\|_2^2 \\
&= 2 - 2\langle U_i, V_i \rangle - (2 - 2\langle U_i, V_j \rangle) \\
&= 2(\langle U_i, V_j \rangle - \langle U_i, V_i \rangle) \\
&\leq 2(-\mathsf{m} + \mathsf{b_{rel}} - \mathsf{m} - \mathsf{b_{rel}}) = -4\mathsf{m}.
\end{aligned}$$

This finishes the proof. $\qquad\square$

B Proof of Theorem 3.5: Dimension vs Size tradeoff

Proof of Theorem 3.5. Let

$$H \sim \mathrm{Unif}(S^{d-1}), \qquad C(H) = \{\, i : \langle c_i, H \rangle > \delta \,\}, \quad N' = |C(H)|,$$

where $c_i = (U_i + V_i)/2$ and $\delta \in (0, 1)$ will be chosen later.

$$\|c_i\|^2 = \frac{1 + \langle U_i, V_i \rangle}{2} \in \left[\tfrac{1+\mathsf{m}+\mathsf{b_{rel}}}{2}, 1\right], \text{ so } \|c_i\| \geq \sqrt{(1 + \mathsf{m} + \mathsf{b_{rel}})/2}$$

Then the inner product satisfies

$$\Pr\big[\langle c_i, H \rangle > \delta\big] = \Gamma_d\Big(\tfrac{\delta}{\|c_i\|}\Big) \; \geq \; \Gamma_d\Big(\delta\sqrt{\tfrac{2}{1+\mathsf{m}+\mathsf{b_{rel}}}}\Big),$$

22

where $\Gamma_d(x) = \Pr[H_1 > x]$ is strictly decreasing in x. By linearity of expectation,

$$\mathbb{E}[N'] \;\geq\; N\,\Gamma_d\!\Big(\delta\sqrt{\tfrac{2}{1+\mathsf{m}+\mathsf{b}_{\mathsf{rel}}}}\Big),$$

so there exists a realization of H with

$$N' \;\geq\; N\,\Gamma_d\!\Big(\delta\sqrt{\tfrac{2}{1+\mathsf{m}+\mathsf{b}_{\mathsf{rel}}}}\Big). \tag{21}$$

Define for the index set $C = C(H)$ the sums

$$U_C = \sum_{i\in C} U_i, \quad V_C = \sum_{i\in C} V_i, \quad x_i = U_i - V_i, \quad x_C = \sum_{i\in C} x_i,$$

and set

$$A_C = \sum_{i\in C}\langle U_i, V_i\rangle, \quad B_C = \sum_{\substack{i,j\in C\\ i\neq j}}\langle U_i, V_j\rangle, \quad \xi_C = \frac{1}{N'}\Big(\sum_{i\in C}\|x_i\|^2\Big) - \|\tfrac{1}{N'}x_C\|^2 \geq 0.$$

A direct expansion shows

$$\|U_C + V_C\|^2 = N'^2(2 - \xi_C) \;-\; 2(N'-2)\,A_C \;+\; 4\,B_C. \tag{22}$$

On the other hand,

$$\Big\|\sum_{i\in C} c_i\Big\| \;=\; \frac{1}{2}\|U_C + V_C\| \;\geq\; \sum_{i\in C}\langle c_i, H\rangle \;>\; N'\delta,$$

so

$$\|U_C + V_C\|^2 > 4N'^2\delta^2. \tag{23}$$

Combining (22) and (23), and using $A_C \geq (\mathsf{m} + \mathsf{b}_{\mathsf{rel}})N'$ and $B_C \leq (\mathsf{b}_{\mathsf{rel}} - \mathsf{m})N'(N'-1)$, yields

$$4N'^2\delta^2 \;\leq\; N'^2(2 - \xi_C) \;-\; 2(N'-2)\,(\mathsf{m} + \mathsf{b}_{\mathsf{rel}})N' \;+\; 4\big[(\mathsf{b}_{\mathsf{rel}} - \mathsf{m})\,N'(N'-1)\big]$$

Which means $N'\big(3\mathsf{m} - 1 + 2\delta^2 - \mathsf{b}_{\mathsf{rel}}\big) \;\leq\; 4\mathsf{m}$. Where in the last reduction we dropped the $\xi_C \geq 0$ term. Hence, whenever $2\delta^2 > 1 - 3\mathsf{m} + \mathsf{b}_{\mathsf{rel}}$,

$$N' \;\leq\; \frac{4\mathsf{m}}{2\delta^2 - (1 - 3\mathsf{m} + \mathsf{b}_{\mathsf{rel}})}. \tag{24}$$

Combine (21) and (24) to get

$$N \;\leq\; \frac{4\mathsf{m}}{2\delta^2 - (1 - 3\mathsf{m} + \mathsf{b}_{\mathsf{rel}})}\;\Gamma_d\!\Big(\delta\sqrt{\tfrac{2}{1+\mathsf{m}+\mathsf{b}_{\mathsf{rel}}}}\Big)^{-1}.$$

Recalling Shannon's asymptotic lower-bound $\Gamma_d(\cos\theta) = \exp\{d\log\sin\theta + o_\theta(d)\}$ [Sha59, (11)] with $\cos\theta = \delta\sqrt{2/(1 + m + \mathsf{b}_{\mathsf{rel}})}$ and correponding $\sin\theta = \sqrt{1 - \cos^2\theta} = \sqrt{1 - \tfrac{1-3\mathsf{m}+\mathsf{b}_{\mathsf{rel}}}{1+\mathsf{m}+\mathsf{b}_{\mathsf{rel}}}}$, the bound is optimized by choosing $\delta = \sqrt{\tfrac{1-3\mathsf{m}+\mathsf{b}_{\mathsf{rel}}}{2}}$. This results in the claimed bound

$$N \leq \exp(-d\log\sin\theta + o_\theta(d)). \qquad\qquad \square$$

C Omitted Proofs from Section 3.3: Combinatorics of The Modality Gap

Here, we analyze configurations $\{(U_i, V_i)\}_{i=1}^N \in (\mathbb{S}^{d-1} \times \mathbb{S}^{d-1})^{\times N}$ with the following property:

$$\begin{aligned}\langle U_i, V_i\rangle > 0 \; \forall i,\\ \langle U_i, V_j\rangle < 0 \; \forall i \neq j.\end{aligned} \tag{25}$$

Ultimately, we aim to prove Theorem 3.6. We also prove several other facts on the way. Our proofs are based on simple facts from convex geometry which we introduce now. One can find more, for example, in the excellent book [BMS12].

C.1 Preliminaries from Convex Geometry

A set $K \subseteq \mathbb{R}^d$ is called *convex* if for any $\alpha \in [0, 1]$ and any $p, q \in K$, it is also the case that $\alpha p + (1 - \alpha)q \in K$. In particular, for any points $p_1, p_2, \ldots, p_k \in \mathbb{R}^d$, the following two sets are convex. The *convex hull* defined by

$$\mathsf{conv}(p_1, p_2, \ldots, p_n) := \left\{ \alpha_1 p_1, \alpha_2 p_2 + \cdots + \alpha_k p_k \ : \ \alpha_i \geq 0 \quad \forall i \text{ and } \sum_{i=1}^n \alpha_i = 1 \right\}$$

and the *convex cone* defined by

$$\mathsf{cone}(p_1, p_2, \ldots, p_n) := \left\{ \alpha_1 p_1, \alpha_2 p_2 + \cdots + \alpha_k p_k \ : \ \alpha_i \geq 0 \quad \forall i \text{ and } \sum_{i=1}^n \alpha_i \leq 1 \right\}$$

$$= \mathsf{conv}(p_1, p_2, \ldots, p_n, 0).$$

We also introduce the dual cone. For a set $S \subseteq \mathbb{R}^n$, the *dual cone* is given by

$$\mathsf{dualcone}(S) := \{ v \in \mathbb{R}^n \ : \ \langle v, x \rangle \geq 0 \quad \forall x \in S \}.$$

We will use the following classic theorems from convex geometry.

Theorem C.1 (Helly [Hel23]). *Let $X_1, X_2, \ldots, X_n$ be a finite collection of convex sets in $\mathbb{R}^d$. If the intersection of every $d + 1$ of these sets is nonempty, then the intersection of all the sets is nonempty. Formally,*

$$\text{If } \bigcap_{i \in I} X_i \neq \emptyset \quad \text{for all } I \subset \{1, 2, \ldots, n\} \text{ with } |I| = d + 1, \text{then } \bigcap_{i=1}^n X_i \neq \emptyset.$$

Theorem C.2 (Carathéodory [Car11, Ste13]). *Let $A \subseteq \mathbb{R}^d$. If $\mathbf{x} \in conv(A)$, then there exists a set $B \subseteq A$ such that $|B| \leq d + 1$ and $\mathbf{x} \in \mathsf{conv}(B)$.*

Theorem C.3 (Hyperplane Separation Theorem [Min10]). *Let X and Y be two nonempty, disjoint convex sets in $\mathbb{R}^d$. Then there exists a nonzero vector $a \in \mathbb{R}^d$ and a scalar b such that*

$$\langle a, x \rangle \leq b \quad \text{for all } x \in X,$$
$$\langle a, y \rangle \geq b \quad \text{for all } y \in Y.$$

C.2 Combinatorics of Modality Gap

Proposition 2. *If (25) hold and $N \geq d + 2$, then there exists some $h \in \mathbb{S}^{d-1}$ such that $\langle h, U_i \rangle > 0$ for all i.*

Proof. For each $i = 1, \ldots, N$, define the open half-space

$$H_i = \{ x \in \mathbb{R}^d : \langle U_i, x \rangle > 0 \}.$$

Each H_i is convex. We first show that any subcollection of $d + 1$ of these half-spaces has nonempty intersection. Indeed, pick distinct indices $i_1, \ldots, i_{d+1}$; since $N \geq d + 2$, there is an index $j \notin \{i_1, \ldots, i_{d+1}\}$. By (25), for each $k = 1, \ldots, d + 1$,

$$\langle U_{i_k}, V_j \rangle < 0 \text{ , so } \langle U_{i_k}, -V_j \rangle > 0,$$

and $-V_j \in \bigcap_{k=1}^{d+1} H_{i_k} \neq \varnothing$.

Since every $d + 1$ of the H_i intersect and $N \geq d + 2$, Helly's theorem implies

$$\bigcap_{i=1}^N H_i \neq \varnothing.$$

Choose any $h_0 \in \bigcap_{i=1}^N H_i$. Then $\langle h_0, U_i \rangle > 0$ for all i. Setting $h = h_0 / \|h_0\| \in \mathbb{S}$ preserves these strict inequalities. $\square$

Proposition 3. *If (25) hold and $N \geq d + 2$, then there exists some $h \in \mathbb{R}^d$ such that $\langle h, U_i \rangle > 0$ for all i and $h \in \mathsf{conv}(U_1, U_2, \ldots, U_N)$.*

Proof. Let $C := \text{conv}(U_1, \ldots, U_N) \subset \mathbb{R}^d$, a compact convex set. Take the unit vector h given by Proposition 2 and denote by h' its projection onto C. This implies the fact that that the hyperplane

$$H := \left\{ x \in \mathbb{R}^d : \langle h - h', \, x - h' \rangle = 0 \right\}$$

supports the set C at the point h': all points of C (hence each U_i) lie in the closed half-space

$$H^- := \left\{ x \in \mathbb{R}^d : \langle h - h', \, x - h' \rangle \le 0 \right\}, \tag{26}$$

whereas h itself belongs to the opposite open half-space $H^+ := \{ x : \langle h - h', \, x - h' \rangle > 0 \}$. Choose an orthonormal basis $\{e_1, \ldots, e_d\}$ with

$$e_1 := \frac{h - h'}{\|h - h'\|}.$$

In these coordinates

$$h = h' + \alpha e_1, \quad \alpha := \|h - h'\| > 0, \qquad h' = 0 \cdot e_1 + h'_\perp,$$

while every U_i has a decomposition $U_i = U_{i,1}\, e_1 + U_{i,\perp}$ with $U_{i,1} \le 0$.

For each i,
$$\langle h', U_i \rangle - \langle h, U_i \rangle = \langle h' - h, \, U_i \rangle = -\alpha\, U_{i,1} \; \ge \; 0.$$

Because $\langle h, U_i \rangle > 0$, we conclude that

$$\langle h', U_i \rangle > 0 \qquad (i = 1, \ldots, N). \tag{27}$$

$\square$

Proof of Theorem 3.6. Let h be the vector provided by Proposition 3, so $h \in \text{conv}(U_1, \ldots, U_N)$ and $\langle h, U_i \rangle > 0$ for every i. Set the cone

$$C' := \text{cone}\{U_1, \ldots, U_N\} = \left\{ \sum_{i=1}^{N} a_i U_i \; : \; a_i \ge 0 \right\}.$$

Because each U_i has positive dot product with h, define the affine hyperplane

$$H := \left\{ x \in \mathbb{R}^d : \langle x, h \rangle = 1 \right\}.$$

Every ray $\{\lambda U_i : \lambda > 0\}$ meets H once, namely at

$$Q_i := \frac{1}{\langle U_i, h \rangle}\, U_i \; \in H.$$

Consequently
$$C' \cap H \; = \; \text{conv}\{Q_1, \ldots, Q_N\}. \tag{28}$$

The the vector $h^\dagger$ in H which is parallel to h. $\langle h^\dagger, h \rangle = 1$, so $h^\dagger$ is h rescaled by a positive scalar. Since $h^\dagger$ also lies in $\text{conv}(U_1, \ldots, U_N) \subset C'$, we have $h^\dagger \in C' \cap H$. The hyperplane H is $(d-1)$–dimensional. By Carathéodory's theorem in $\mathbb{R}^{d-1}$, there is a subset $S \subset \{1, \ldots, N\}$ with $|S| \le d$ and weights $\lambda_i \ge 0$, $\sum_{i \in S} \lambda_i = 1$, such that

$$h^\dagger \; = \; \sum_{i \in S} \lambda_i\, Q_i \; = \; \sum_{i \in S} \lambda_i\, \frac{U_i}{\langle U_i, h \rangle}. \tag{29}$$

Fix $k \notin S$. Using Theorem C.2 and (25),

$$\langle h^\dagger, V_k \rangle = \sum_{i \in S} \lambda_i\, \frac{\langle U_i, V_k \rangle}{\langle U_i, h \rangle} < 0,$$

because each numerator $\langle U_i, V_k \rangle$ is negative and each denominator $\langle U_i, h \rangle$ is positive. Hence $\langle h^\dagger, V_k \rangle < 0$ for every $k \notin S$. Only the (at most) d indices in S may give a non–negative value. Note that $h^\dagger$ is already on the unit circle. $\square$
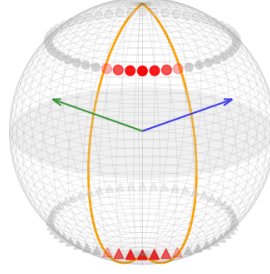
Figure 13: Construction in 3D.

Now we prove that there is a construction for which this bound is almost tight and we can separate all but at least $d-1$ vectors with a hyperplane.

Construction 3 (Tightness of Theorem 3.6). *There exists a set of vectors $\{(U_i, V_i)\}_{i=1}^N$ such that $\langle U_i, V_i \rangle > 0$ for each i, $\langle U_i, V_j \rangle < 0$ for each $i \neq j$, and for any $h \in \mathbb{S}^{d-1}$, at least for $d-1$ values of i, it holds that $\langle h, U_i \rangle$ and $\langle h, V_i \rangle$ have the same sign.*

Proof. For the construction for $d = 3$, note that we can take two parallel k-gons equally far from the equator of the sphere such that the zeniths of their points for one of them is $\pi/4 + \delta$ and for the other one is $3/4\pi - \delta$ and by taking $\delta \to 0$ we can ensure that the dot product between corresponding pairs is positive and the dot product between non-matching pairs is negative. Now note that by taking k sufficiently large and the δ sufficiently small. The intersection of that configuration with the wedge with dihedral angle α contains at least $N-2$ points from one of the k-gons (the U's) and $N-2$ points from the other (the V's) for any value of α. See Fig. 13.

Label those as
$$U_1, \ldots, U_{N-2} \quad \text{and} \quad V_1, \ldots, V_{N-2}.$$
Finally place two more pairs on the equator:
$$U_{N-1} = V_{N-1}, \quad U_N = V_N$$
chosen so that $\langle U_{N-1}, U_N \rangle < 0$ and both make negative dot-products with each wedge boundary ray. This completes the $d = 3$ example.

For the general case ($d > 3$). Let $\omega_1, \ldots, \omega_{d+1}$ be the vertices of a regular simplex in $\mathbb{R}^d$. Set
$$U_i = V_i = \omega_i, \quad i = 1, \ldots, d-3.$$

These occupy a $(d-3)$–dimensional subspace. In the orthogonal complement (which is 3–dimensional), embed the $d = 3$ construction, obtaining pairs $(U_{d-2}, V_{d-2}), \ldots, (U_N, V_N)$. Finally, pick a small $\varepsilon > 0$ and renormalize:
$$U_i' = \varepsilon\,\omega_{d-2} + \sqrt{1 - \varepsilon^2}\,U_i, \quad V_i' = \varepsilon\,\omega_{d-2} + \sqrt{1 - \varepsilon^2}\,V_i, \quad i = d-2, \ldots, N.$$

For ε sufficiently small, all the required dot-product signs are preserved, and since the configuration was orthogonal to U_i for $i = 1, 2, \ldots, d-3$,
$$\langle U_i, V_j \rangle = -\epsilon\frac{1}{d} < 0, \forall i = 1, 2, \ldots, d-3, j = d-2, d-1, \ldots, N,$$
as needed. $\qquad\square$

Proposition 4. *If (25) hold then $U_i \notin \mathrm{cone}(\{U_j\}_{j \neq i})$ for any i.*

Proof. Suppose, to the contrary, that for some fixed i there exist scalars $a_j \geq 0$ for $j \neq i$ such that

$$U_i = \sum_{j \neq i} a_j U_j.$$

Taking the inner product with V_i gives

$$\langle V_i, U_i \rangle = \sum_{j \neq i} a_j \langle V_i, U_j \rangle.$$

Since by (25) we have $\langle V_i, U_j \rangle < 0$ for all $j \neq i$ and each $a_j \geq 0$, the right–hand side is nonpositive. But the left–hand side is strictly positive, a contradiction. Therefore $U_i \notin \mathsf{cone}(\{U_j\}_{j \neq i})$. $\square$

Proposition 5. *If $d = 2$ and $N \geq 4$, there does not exist a configuration satisfying* (25).

Proof. Because $N \geq d + 2$, Proposition 3 gives a unit vector h with $\langle h, U_i \rangle > 0$ for every i. Rotate so $h = (1, 0)$; all U_i now lie in the open right half-plane $x > 0$. Write their polar angles in $\left(-\frac{\pi}{2}, \frac{\pi}{2}\right)$ as

$$-\frac{\pi}{2} < \theta_1 < \theta_2 < \cdots < \theta_N < \frac{\pi}{2}.$$

Now note that $U_2 \in \mathsf{cone}(U_1, U_3)$ which is a contradiction by Proposition 4. Therefore configuration (25) cannot exist when $d = 2$ and $N \geq 4$. $\square$

D   Further Experiments and Experimental Details

For the experiments in Section D.1, we used a single A100 GPU. All other experiments are done on a standard CPU and take at most several minutes.

D.1   Experiments on ImageNet

In Figures 1 and 3, we performed experiments on real data with the SigLIP implementation. While a next generation vision-language encoder was introduced with the SigLIP 2 paper [TGW$^+$25a], we opted to use the original SigLIP model rather than SigLIP 2 because SigLIP 2's enhanced training recipe – incorporating auxiliary decoder, self-distillation, and masked-prediction losses – would confound our ability to isolate the impact of the core Sigmoid Contrastive Loss on the embeddings. The data we used is the validation dataset of ImageNet which contains 50000 captioned images with 1000 distinct captions. We used 8 trained models listed in Table 1 which can all be downloaded from Hugging Face.

Figure 14: "African chameleon" on the right and "American chameleon" on the left from the ImageNet validation dataset. The B/16 model representation of the image of "American chameleon" was closer to the representation of the word African chameleon than that of American chameleon

We embedded all images and labels in the validation set using the B/16 model. We used PIL to resize all images to 224x24. In Figure 1, we show in red the inner products between wrong image-caption pairs and in blue between correct image-caption pairs.

As we point out, the inner product separation is nearly satisfied. There are some errors, but such are expected. For example, we discovered that the best matching image embeddings picture of the word "African chameleon" was "American chameleon". Both are species of chameleon and, hence, the images similar, such errors are to be expected in practice. For large models, the reported accuracy on ImageNet in [ZMKB23b] is 84.5%.

D.2   Experiments with Locked Representation

In Figure 4, we performed experiments in which one modality is fixed. Namely, we first draw $\{U_i\}_{i=1}^{N}$ uniformly on the sphere and then fix them. Then, we try to synchronize with $\{V_i\}_{i=1}^{N}$ by running gradient descent on the respective loss function. Specifically, we have experiments on:

- *Fixed Low Temperature $t = 200$ and bias $b = 0$.* We fix $t = 200, b = 0$ and run Adam on $\{V_i\}_{i=1}^N$ for the loss $\mathcal{L}^{\mathsf{Sig}}(\{U_i\}_{i=1}^N, \{V_i\}_{i=1}^N; t, b)$ and initial learning rate 0.01.

- *Fixed High Temperature $t = 10$ and bias $b = 0$.* We fix $t = 10, b = 0$ and run Adam on $\{V_i\}_{i=1}^N$ for the loss $\mathcal{L}^{\mathsf{Sig}}(\{U_i\}_{i=1}^N, \{V_i\}_{i=1}^N); t, b$ and initial learning rate 0.01.

- *Trainable Temperature and Bias.* We initialize at $t = 10 = e^{t'}, b = 0$ and run Adam with on $\{V_i\}_{i=1}^N, t', b$ for the loss $\mathcal{L}^{\mathsf{Sig}}(\{U_i\}_{i=1}^N, \{V_i\}_{i=1}^N; e^{t'}, b)$ and initial learning rate 0.01. We note that all of our trainable experiments are with the parametrization $t = e^{t'}$ which ensures positive temperature as in [ZMKB23b].

- *Trainable Temperature and Relative Bias.* We initialize at $t = 10 = e^{t'}, b = 0$ and run Adam on $\{V_i\}_{i=1}^N, t', \mathsf{b}_{\mathsf{rel}}$ for the loss $\mathcal{L}^{\mathsf{RB-Sig}}(\{U_i\}_{i=1}^N, \{V_i\}_{i=1}^N; e^{t'}, \mathsf{b}_{\mathsf{rel}})$ and initial learning rate 0.01. We note that all of our trainable experiments are with the parametrization $t = e^{t'}$ which ensures positive temperature as in [ZMKB23b].

The specific experiment in Fig. 10 is for $d = 10, N = 100$. We also note that we did one more comparison, which is not reported in the main paper – with an explicit adapter from Figure 4. Namely:

- *Trainable Temperature and Relative Bias with Explicit Adapter.* We initialize at $t = 10 = e^{t'}, b = 0, \delta = \frac{e^x}{1+e^x}$ with $x = 1/2$ and run Adam on $\{V_i\}_{i=1}^N, t', \mathsf{b}_{\mathsf{rel}}, x$ for the loss $\mathcal{L}^{\mathsf{RB-Sig}}(\{\mathsf{A}^\delta_{\mathsf{locked}}(U_i)\}_{i=1}^N, \{\mathsf{A}^\delta_{\mathsf{trainable}}(V_i)\}_{i=1}^N; e^{t'}, \mathsf{b}_{\mathsf{rel}})$ and initial learning rate 0.01. Since the adapter is an invertible transformation on the representations, we reported the inner products both with the adapter and without it (that is, we invert by removing the last coordinate and dividing by δ.)
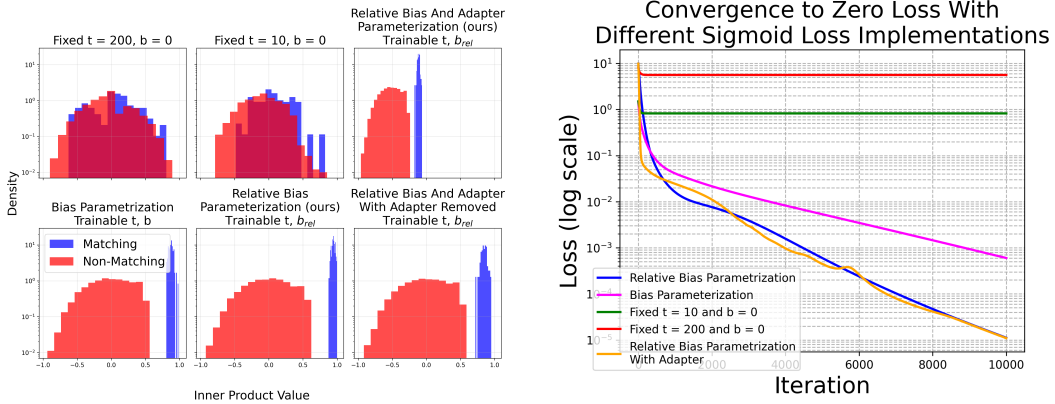

Figure 15: Inner-product separation and loss convergence under six sigmoid-loss parameterizations. *Left:* Log-density histograms of inner-product scores for matching (blue) versus non-matching (red) pairs, evaluated under fixed inverse temperature $t = 200, b = 0$, fixed $t = 10, b = 0$, trainable bias b, our relative-bias parameterization (trainable $\mathsf{b}_{\mathrm{rel}}$), and the same two schemes with the adapter removed; only the trainable-bias models show clear separation. *Right:* Sigmoid-loss trajectories (log scale) over 10,000 iterations for the same six settings; only those variants that learn both bias and inverse temperature reach zero loss, and our relative-bias parameterization (with and without adapter) converges most rapidly.

We can overall see that the performance of $\mathcal{L}^{\mathsf{RB-Sig}}$ algorithm with an adapter and without is rather comparable and the inner product separations are similar. One difference to note is that the training with adapter seems less stable. Thus, we believe that in practice not using the adapter might be the better approach.

D.3 Experiments with Multiple Modalities

In Figure 11, we performed experiments with $k = 4$ modalities. Namely, we synchronize $\{(U_i^{(1)}, U_i^{(2)}, U_i^{(3)}, U_i^{(4)})\}_{i=1}^N$ by running gradient descent on the sums of all pairwise loss functions between the 4 modalities. Specifically, we have experiments on:

- *Fixed Low Temperature $t = 200$ and bias $b = 0$.* We fix $t = 200, b = 0$ and run Adam on $\{V_i\}_{i=1}^N$ for the loss $\mathcal{L}^{\mathsf{Sig}}(\{U_i\}_{i=1}^N, \{V_i\}_{i=1}^N; t, b)$ and initial learning rate 0.01.

- *Fixed High Temperature $t = 10$ and bias $b = 0$.* We fix $t = 10, b = 0$ and run Adam on $\{V_i\}_{i=1}^N$ for the loss $\mathcal{L}^{\mathsf{Sig}}(\{U_i\}_{i=1}^N, \{V_i\}_{i=1}^N); t, b$ and initial learning rate 0.01.

- *Trainable Temperature and Bias.* We initialize at $t = 10 = e^{t'}, b = 0$ and run Adam with on $\{V_i\}_{i=1}^N, t', b$ for the loss $\mathcal{L}^{\mathsf{Sig}}(\{U_i\}_{i=1}^N, \{V_i\}_{i=1}^N; e^{t'}, b)$ and initial learning rate 0.01. We note that all of our trainable experiments are with the parametrization $t = e^{t'}$ which ensures positive temperature as in [ZMKB23b].

- *Trainable Temperature and Relative Bias.* We initialize at $t = 10 = e^{t'}, b = 0$ and run Adam on $\{V_i\}_{i=1}^N, t', \mathsf{b}_{\mathsf{rel}}$ for the loss $\mathcal{L}^{\mathsf{RB-Sig}}(\{U_i\}_{i=1}^N, \{V_i\}_{i=1}^N; e^{t'}, \mathsf{b}_{\mathsf{rel}})$ and initial learning rate 0.01. We note that all of our trainable experiments are with the parametrization $t = e^{t'}$ which ensures positive temperature as in [ZMKB23b].

The specific experiment in Fig. 11 is for $d = 10, N = 100$.

We ran additional experiments to investigate how increasing the number of modalities k affects the final separation margin. With trainable temperature and relative bias, we observe that the margin generally increases as we synchronize more modalities, as summarized in Table 3. This suggests that training with more modalities may lead to more robust representations, as a larger margin implies better separation between matching and non-matching pairs.

Table 3: Final margin as a function of the number of modalities being synchronized. The experiment was run with $N = 100$ and $d = 10$.

Number of Modalities	Final Margin
2	0.471241
4	0.427528
6	0.472571
8	0.595576
14	0.610853
20	0.611314

D.4 Bias Parameterization Leads to Zero Relative Bias

Finally, we do experiments to show that training with $\mathcal{L}^{\mathsf{Sig}}$ leads to near zero relative bias, as in [ZMKB23a]. We compare with $\mathcal{L}^{\mathsf{RB-Sig}}$. Concretely, we run experiments with $N = 100$ points $\{(U_i, V_i)\}_{i=1}^N$ initialized at random and run Adam on $\mathcal{L}^{\mathsf{Sig}}(\{(U_i, V_i)\}_{i=1}^N; t, b)$, respectively $\mathcal{L}^{\mathsf{RB-Sig}}(\{(U_i, V_i)\}_{i=1}^N; t, \mathsf{b}_{\mathsf{rel}})$, for 10000 epochs starting at $t = 10$ and varying biases.

We compare the evolution of relative biases, inverse temperature, loss function, and margins of the final configuration.

Finally, we also compare the margins. The reason is that as we know from Theorem 3.4, there is an important relationship between relative bias and margin. The fact that embeddings trained with $\mathcal{L}^{\mathsf{RB-Sig}}$ have a larger relative bias also impacts the margin.

D.5 Initializing Fixed Relative Bias

We verify this with an experiment where we initialize representations uniformly at random, fix the relative bias $\mathsf{b}_{\mathsf{rel}}$, and train the representations and inverse temperature t using Adam. As shown in Table 4, choosing $\mathsf{b}_{\mathsf{rel}} \approx 0.7$ yields the largest final margin, while other choices result in smaller
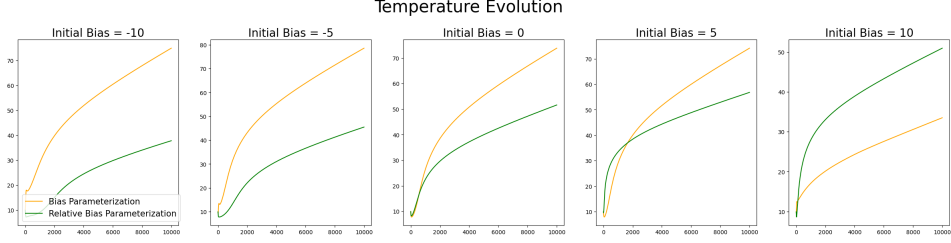
Figure 16: Evolution of the inverse temperature parameter during the training process.
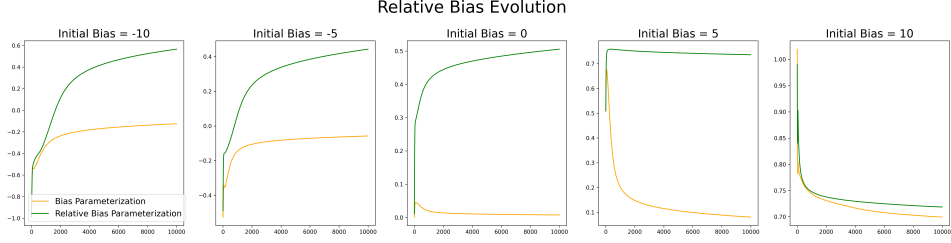

Figure 17: Relative bias is in general smaller when training with the $\mathcal{L}^{\mathsf{Sig}}$ parameterization. In general, it converges to zero and is significantly smaller than the relative bias of the $\mathcal{L}^{\mathsf{RB-Sig}}$.
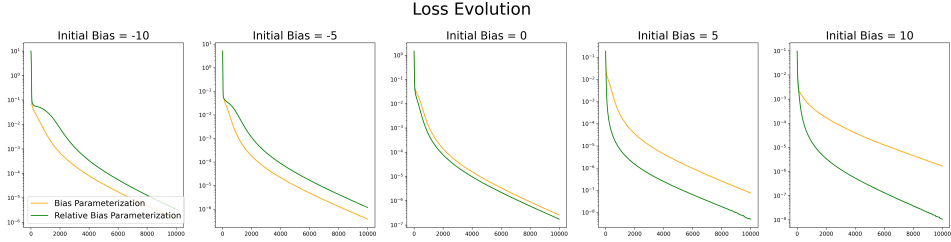

Figure 18: In general, the loss converges faster to zero when trained with the $\mathcal{L}^{\mathsf{RB-Sig}}$ parameterization than when trained with $\mathcal{L}^{\mathsf{Sig}}$.
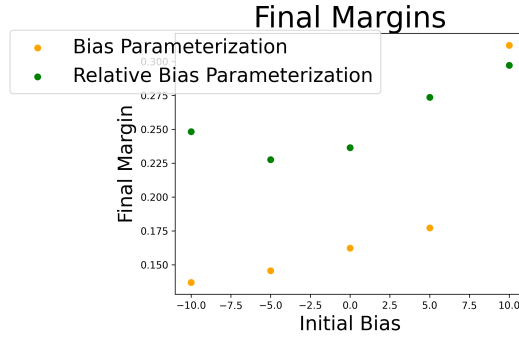

Figure 19: In general, the margin is much larger for representations trained with the $\mathcal{L}^{\mathsf{RB-Sig}}$ parameterization. As we know from 1, this means that they are more robust on retrieval tasks.

margins. This confirms that the relative bias parameter can effectively steer the optimization towards configurations with desirable properties.

D.6 Initializing Learnable Temperature and Relative Bias.

We investigated the effect of initial temperature t and relative bias $\mathsf{b_{rel}}$ on the final margin. We ran a hyperparameter search and found that the final margin is best for a small initial temperature ($t \leq 3$) or an intermediate temperature ($t \approx 10$) with a relatively large initial relative bias ($\mathsf{b_{rel}} \approx 0.6$). The

30

Table 4: Final margin and loss for different fixed values of relative bias b_{rel}. Training is performed on the representations and inverse temperature t. The largest margin is achieved for $b_{rel} \approx 0.7$.

Fixed Relative Bias	Final Temperature	Achieved Margin	Final Loss
-1.00	6.961601	-0.000001	0.693150
-0.90	56.188858	-0.000000	0.009245
-0.80	23.300198	-0.000000	0.014105
-0.70	162.664841	0.092437	0.000005
-0.60	125.656731	0.122326	0.000003
-0.50	104.095329	0.152893	0.000003
-0.40	90.788620	0.182992	0.000002
-0.30	81.079422	0.213618	0.000001
-0.20	75.061546	0.242438	0.000001
-0.10	71.254242	0.273600	0.000000
0.00	69.018265	0.301340	0.000000
0.10	69.534515	0.329022	0.000000
0.20	67.996437	0.353406	0.000000
0.30	61.796310	0.390087	0.000000
0.40	55.452553	0.430921	0.000000
0.50	48.406261	0.466707	0.000000
0.60	44.391388	0.498564	0.000000
0.70	42.265457	0.527834	0.000000
0.80	37.361767	0.539749	0.000001
0.90	33.167175	0.483351	0.000036
1.00	23.817665	0.513416	0.000693

results, summarized in Table 5, show that while the optimization is robust to a range of initializations, a poor choice (e.g., high initial t and low b_{rel}) can lead to suboptimal final representations with a small or even negative margin.

Table 5: The final margin achieved for different initializations of temperature (Temp) and relative bias (b_{rel}). The best results (bolded) are obtained with low-to-intermediate temperature and high relative bias.

Temp	-1.0	-0.8	-0.6	-0.4	-0.2	0.0	0.2	0.4	0.6	0.8	1.0
1	0.567	0.567	0.566	0.564	0.566	0.566	0.565	0.568	0.570	**0.574**	0.573
3	0.545	0.543	0.526	0.499	0.483	0.488	0.536	0.563	0.570	**0.574**	0.573
10	0.439	0.425	0.415	0.406	0.402	0.410	0.429	0.524	0.566	0.547	0.562
30	0.301	0.297	0.294	0.315	0.343	-0.942	-0.915	-0.935	-1.171	-1.051	-1.145
100	-0.774	-0.679	-0.483	-0.740	-0.878	-0.956	-0.978	-1.109	-1.186	-1.080	-1.449

E   Connection to Linear Representation Hypothesis Across Modalities

It has been observed by many authors that modern dense embedding spaces acquire correspondence between linear-algebraic operations and real-world concepts. This has been immortalized as "King - Man + Woman $\approx$ Queen" in word2vec [MCCD13] and is also observed in modern LLMs as well [PCV24, TCM$^+$24]. Curiously, we find that contrastive pretraining with sigmoid loss also leads to a special case of LRH: there emerges a direction $\bar{x}$ such that adding it to an image embedding (almost) recovers the embedding of a matching text caption. Indeed, looking at the optimal embeddings in Fig. 5 we can see that $U_i - V_i$ does not depend on i, which we take as a manifestation of LRH in this context (the concept being "shift text to image" or more generally one modality to another). Furthermore, both our upper and lower bounds on the cardinality of the embeddings in Section 3.2 require Cross-Modality-LRH satisfying configurations to be tight.

In the proof of Theorem 3.5 in Section B we defined the following quantity characterizing an arbitrary constellation

$$\xi = \frac{1}{N}\left(\sum_i \|x_i\|^2\right) - \|\bar{x}\|^2 \geq 0\,,$$

where $x_i = U_i - V_i$ and $\bar{x} = \frac{1}{N}\sum_i x_i$. (In the proof ξ was defined for a carefully chosen sub-constellation). We note that the upper bound in that Theorem 3.5 could only possibly be tight if $\xi \approx 0$. In this section we will further show that ξ can be used as a quantitative measure of the degree to which *Linear Representation Hypothesis* is satisfied.

First, let us establish that when ξ is small (as $\xi \geq 0$ is used in the proof of Theorem 3.5 this means that the bounds in that proof are tight). More importantly, a small ξ implies something significant about our representations: it suggests that the difference vector, $U_i - V_i$, is nearly identical for all indices i. Think of it this way: if you have two sets of learned representations, say U_i for images and V_i for their corresponding text descriptions, a small ξ means that you can apply a consistent shift (a single vector) to all the V_i vectors to transform them into their corresponding U_i vectors. So, by shifting a text representation, you could get its corresponding image representation.

Proposition 6. *If $\xi = o(1)$ then $\frac{1}{N}\sum_{i=1}^N \|x_i - \bar{x}\|^2 = o(1)$ and all pairs of representations align in the sense that $U_i - V_i \approx U_j - V_j$ for all i, j. In particular, the U's are obtained from the V's by adding a vector $\bar{x}$, which thus serves as a concept shift.*

Proof. A simple algebra shows that ξ has the following two equivalent expressions:

$$\xi = \frac{1}{N}\sum_{i=1}^N \|x_i - \bar{x}\|^2 = \frac{1}{2N^2}\sum_{i,j=1}^N \|x_i - x_j\|^2\,.$$

Thus, the statement "$\xi = o(1)$" is equivalent to

$$0 \leq \frac{1}{N}\sum_{i=1}^N \|x_i - \bar{x}\|^2 \to 0\,,$$

which in turn implies that $U_i - V_i \approx \bar{x}$ simultaneously for all i. The argument for $U_i - V_i \approx U_j - V_j$ is similar. $\square$

Corollary 2. *If $\xi = 0$, then $U_i - V_i$ are all identical for all indices i.*

Indeed, in Fig. 20 when training directly the representations, we can observe the ξ value converging to 0 for a range of different dimensions.
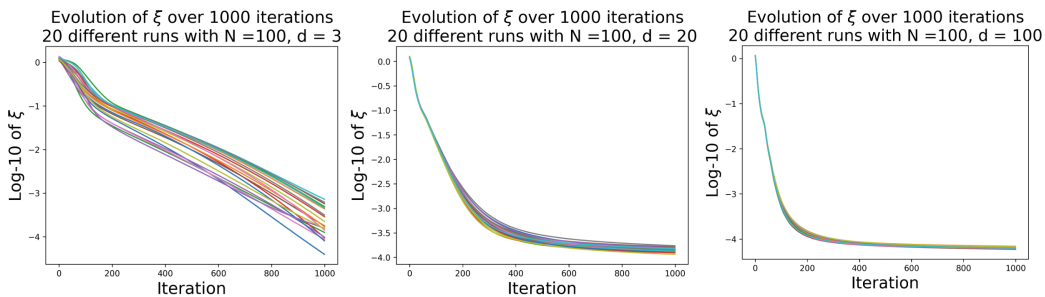

Figure 20: Convergence of the value of ξ to zero during an experiment with $d = 10$ and 100 U_i, V_i pairs trained with SigLIP.

However, the value of ξ for real models is far from 0 on the ImageNet validation dataset. Our intuition for this is that the dimension used $d \approx 1000$ is far from optimal, hence $\xi = 0$ is not required. It is an interesting open direction whether we can train models in lower dimension utilizing the fact that $\xi \longrightarrow 0$ in that case. For example, one can explicitly add ξ in the loss function.

Model	ξ	Mean of Norms	Norm of Mean	Random Mean of Norms
siglip-so400m-patch14-384	0.6086	1.7249	1.1162	2.0029
siglip-base-patch16-224	0.5880	1.8100	1.2221	2.0609
siglip-base-patch16-384	0.5908	1.8068	1.2160	2.0631
siglip-large-patch16-256	0.5535	1.7955	1.2420	2.0711
siglip-so400m-patch14-224	0.6207	1.7270	1.1063	2.0038
siglip-base-patch16-256	0.5767	1.7991	1.2225	2.0588
siglip-base-patch16-512	0.5908	1.8059	1.2151	2.0644
siglip-large-patch16-384	0.5744	1.8084	1.2340	2.0762

Table 6: ξ for different SigLIP models in ImageNet validation. We plot respectively ξ, $\frac{1}{N}\left(\sum_i \|x_i\|^2\right)$ as mean of norms, $\|\bar{x}\|^2$ as norm of mean, $\frac{1}{N}\left(\sum_i \|U_i - V_{\pi(i)}\|^2\right)$ as random mean of norms where π is a uniformly random permutation. We can see that the mean of norms is closer to the random mean of norms (i.e., random pairing of text-images, not corresponding to the ground truth) rather than the norm of means, which would imply $\xi \longrightarrow 0$.